Available online at www.sciencedirect.com

ScienceDirect

Geochimica et Cosmochimica Acta 161 (2015) 50–70

Geochimica et Cosmochimica Acta

www.elsevier.com/locate/gca

Sources, sinks and long-term cycling of iodine in the hyperarid Atacama continental margin

Fernanda Álvarez [a,b,*], Martin Reich [a,b], Alida Pérez-Fodich [a,b], Glen Snyder [c,d], Yasuyuki Muramatsu [e], Gabriel Vargas [a,b], Udo Fehn [f]

[a] *Department of Geology, Universidad de Chile, Santiago, Chile*
[b] *Andean Geothermal Center of Excellence (CEGA), Universidad de Chile, Santiago, Chile*
[c] *Department of Earth Science, Rice University, Houston, TX 77005, USA*
[d] *Gas Hydrate Research Laboratory, Meiji University Global Front, Tokyo 101-8301, Japan*
[e] *Department of Chemistry, Gakushuin University, Tokyo 113-0033, Japan*
[f] *Department of Earth and Environmental Sciences, University of Rochester, Rochester, NY 14627, USA*

Received 10 March 2014; accepted in revised form 28 March 2015; available online 7 April 2015

Abstract

The Atacama region in northern Chile hosts the driest desert on Earth and is the world's premier iodine production province. The origin of iodine enrichment in Atacama is controversial and fundamentally different processes have been invoked over the years that involve marine, eolian and more recently deep sedimentary fluid and groundwater sources. As a result of the very limited geochemical iodine data in Atacama and the western South American margin, the origin of iodine enrichment in this region still remains elusive. In this study, we present a comprehensive survey of iodine concentrations and isotopic ratios ($^{129}I/I$) of different reservoirs in the Atacama Desert of northern Chile, including nitrate soils, supergene copper deposits, marine sedimentary rocks, geothermal fluids, groundwater and meteoric water. Nitrate soils along the eastern slope of the Coastal Cordillera are found to have mean iodine concentrations of at least three orders of magnitude higher than the mean crustal abundances of ~0.12 ppm, with a mean concentration of ~700 ppm. Soils above giant copper deposits in the Central Depression are also highly enriched in iodine (100's of ppm range), and Cu-iodide and iodate minerals occur in the supergene enrichment zones of some of these deposits. Further east in the Precordillera, Jurassic sedimentary shales and limestones show above-background iodine concentrations, the latter averaging ~50 ppm in the southern portion of the study area. The highest iodine concentrations in fluids were measured in groundwater below nitrate soils in the Coastal Range (~3.5–10 ppm) and in geothermal waters (1–3 ppm) along the volcanic arc. Although highly variable, the iodine isotopic ratios ($^{129}I/I$) of Jurassic marine sedimentary rocks (~300–600 $\times 10^{-15}$), nitrate soils (~150–1500 $\times 10^{-15}$) and waters (~215 $\times 10^{-15}$) are consistently low (<1500 $\times 10^{-15}$), indicating that recent anthropogenic additions are almost negligible in most surficial and deeper reservoirs. Geochemical mixing models reveal that the measured $^{129}I/I$ ratios in Atacama are in agreement with multiple sources of iodine that include variable contributions from old organic iodine sources (*i.e.*, marine sedimentary rocks) and younger fluids such as pore waters, geothermal fluids and meteoric waters. Our results show that the large variation observed in the iodine isotopic ratios of different reservoirs ($^{129}I/I$ from 150 to 1580 $\times 10^{-15}$) is indicative of significant mixing and circulation of fluids of meteoric, sedimentary and volcanic origin along the Chilean continental margin in the last 30 million years. We conclude that this protracted and large-scale fluid flow was driven by tectonic uplift and highly influenced by the climatic history of the Atacama Desert. The combination of such factors has played an unforeseen role in transporting and accumulating

* Corresponding author at: Department of Geology, Universidad de Chile, Plaza Ercilla 803, Santiago, Chile. Tel.: +56 229780627.
E-mail address: fernanda.alvarez.a@gmail.com (F. Álvarez).

http://dx.doi.org/10.1016/j.gca.2015.03.032

iodine and other soluble components in the Atacama region, and is evidence that elemental remobilization is a key process in the overall crustal cycle of iodine over scales of millions of years.

1. INTRODUCTION

The global distribution of iodine (I) is dominated by the marine system, in particular marine sediments, which hold about 70% of the total iodine in the crust at concentrations from 1600 to 10,000 μM (Wong, 1991; Muramatsu and Wedepohl, 1998). In contrast, seawater contains only 0.4 μM due to extensive iodine partition into marine phytoplankton and algae, and subsequent accumulation in marine sediments (Broecker and Peng, 1982; Ullman and Aller, 1983, 1985; Küpper et al., 2008).

Although the global iodine budget and its distribution in marine settings has been generally constrained (Fehn et al., 1986, 2007a), naturally elevated iodine concentrations in rocks, soils and waters are rarely reported, with iodine mineral occurrences being restricted to hyper-arid desert environments. Among these, the Atacama Desert in northern Chile hosts mineral deposits with some of the highest iodine concentrations known in continental settings (Ericksen, 1981). In the Atacama region, iodine is highly concentrated in nitrate soils, a ~1 m thick layer that covers an almost continuous 700 km long by 20 km wide area along the western margin of the Central Depression. Iodine in the nitrates exceeds by 3–4 orders of magnitude the average crustal concentrations and forms iodate (IO_3^-) minerals that occur along with nitrates, sulfates, chlorides and rare perchlorates and chromates (Ericksen, 1981; Muramatsu and Wedepohl, 1998; Pérez-Fodich et al., 2014). In addition, recent studies suggest that iodine enrichment in the region is more widespread than previously thought. For example, high iodine occurrences have been reported in copper deposits from the Coastal Range (*e.g.*, Mantos de la Luna) to the Central Depression (*e.g.*, Spence) and the Precordillera (*e.g.*, Chuquicamata and Escondida). These anomalous iodine concentrations are restricted to supergene zones and soils above copper deposits, forming fine-grained iodides and iodates that coexist with Cu-chlorides and sulfates, among other oxidized Cu phases (Jarrell, 1939, 1944; Reich et al., 2009a, 2013; Cameron et al., 2010).

Recently, Pérez-Fodich et al. (2014) reported $^{129}I/I$ isotopic ratios of iodine-rich nitrate soils from Atacama (~150–600 × 10^{-15}) revealing signatures similar to marine sedimentary pore waters (~200–500 × 10^{-15}; Fehn et al., 2007b). These surprisingly low $^{129}I/I$ ratios are strong evidence for a non-atmospheric source for the iodine component of nitrates and point toward a significant role of groundwater and deep sedimentary fluids in the formation of iodine-bearing nitrate soils in Atacama.

Despite these recent advances, little is known about the regional setting and distribution of iodine in the Atacama Desert. In fact, a survey of previously published studies suggest that iodine enrichment is not exclusively restricted to discrete reservoirs (*e.g.*, nitrate soils and supergene copper deposits), but is rather wide-spread in most surficial reservoirs in Atacama such as surface and ground water, spring and thermal water, and marine sedimentary rocks outcropping between the Central Depression and the Precordillera. Considering the fact that the cycling of iodine is still poorly understood in continental settings, the convergence of anomalous iodine occurrences with unique geologic, tectonic and climatic factors in Atacama offers an intriguing opportunity to investigate iodine enrichment over long timescales in an active continental margin.

In this study, we present a comprehensive survey of iodine concentrations and isotopic ratios ($^{129}I/I$) of selected reservoirs in the Atacama Desert of northern Chile, including nitrate soils, supergene copper ores, sedimentary rocks, geothermal fluids, groundwater and surface water. By coupling new iodine concentration data and $^{129}I/I$ isotopic ratios with previously published data, we show that iodine is significantly enriched in most surface reservoirs, and its origin can be related to multiple sources that include marine sedimentary rocks, geothermal/volcanic fluids and meteoric water. We also explore the role of groundwater as a transport agent in the region, and by using geochemical mixing models, we show that the iodine $^{129}I/I$ ratios can be used not only to trace the origin of iodine, but also to constrain the timescales of groundwater circulation over scales of millions of years.

2. BACKGROUND

2.1. Geological setting

The study area is located in the central Atacama region of northern Chile (19° 20′ S–24° 10′ S), and covers a portion of the Tarapacá and Antofagasta regions (Fig. 1A). The present tectonic configuration of the Chilean active margin is characterized by the subduction of the Nazca Plate beneath the South American Plate (Fig. 1A). This configuration was acquired after the breakup of the Farallon Plate into the Nazca and the Cocos Plates around 25 Ma ago (Pardo-Casas and Molnar, 1987). Currently, the convergence rate between Nazca and South American plates is 7.8 cm/yr in this region, and the sediment column on the under-riding plate includes from the oldest to recent age sediments at the top (DeMets et al., 1994; Angermann et al., 1999).

The uplift history of the northern Chilean Andes has been subject of debate, with two opposing end member models: a rapid rise in elevation in the past 10 Ma (of ~2.5 km at ~10–6 Ma, Garzione et al., 2008) and a slow and steady rise to present elevations since ~60 or 40 Ma (*e.g.*, Barnes and Ehlers, 2009; Charrier et al., 2013 and references within). However, both views are in agreement with the fact that

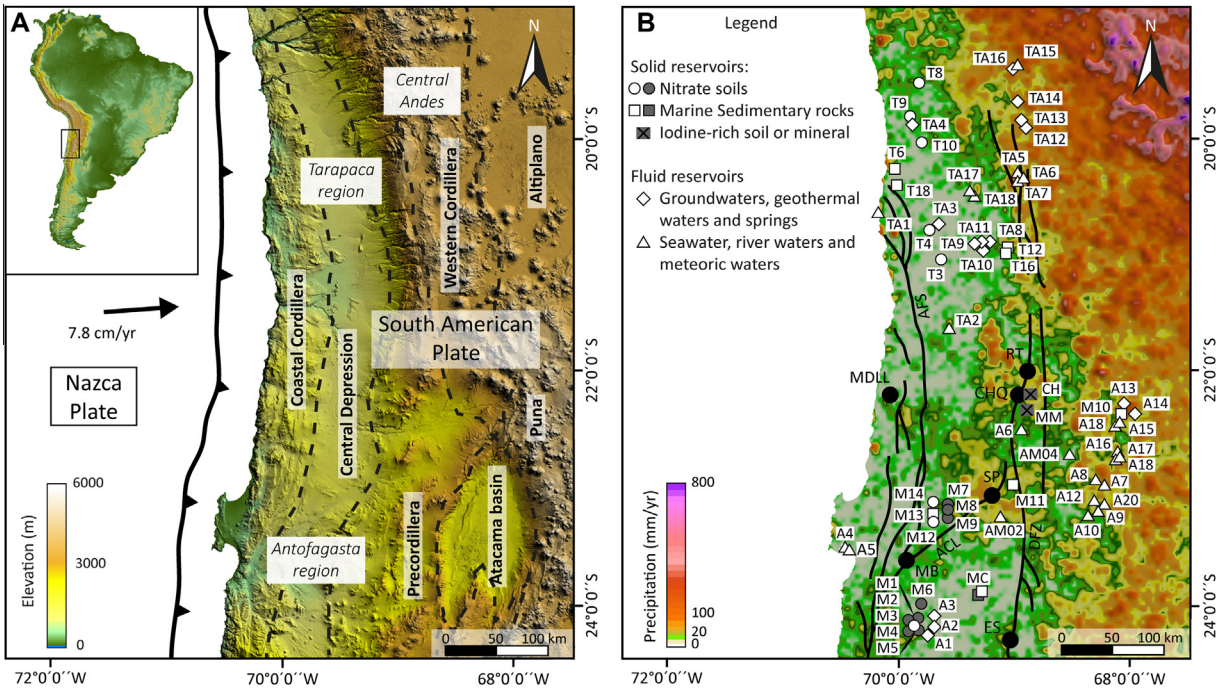

Fig. 1. Map of the studied area: (A) Digital elevation map of northern Chile showing the main morphological units. (B) Mean-annual precipitation map of northern Chile, Puna and Altiplano, showing the distribution of sampling sites used for this study, data points in gray were sampled in previous works (Table 1). The major structural features shown are the Atacama Fault System (AFS), the Antofagasta-Calama Lineament (ACL) and the Domeyko Fault Zone (DFZ). Solid black circles show the location of supergene Cu deposits where high-iodine concentrations have been reported (MDLL: Mantos de la Luna, RT: Radomiro Tomic, CHQ: Chuquicamata, SP: Spence, MB: Mantos Blancos, ES: Escondida).

the Central Andean Cordillera is the result of protracted shortening and thickening over the past ~50 Ma.

In the central Atacama region, four different morphostructural units are identified from west to east: Coastal Cordillera, Central Depression, Precordillera (Domeyko Range) and Western Cordillera (Fig. 1A). The Coastal Cordillera is mainly composed of Jurassic andesitic and Cretaceous sedimentary rocks that are intruded by Jurassic and Lower Cretaceous plutonic rocks (Coira et al., 1982; Marinovic et al., 1995). The Central Depression is mostly covered by Neogene alluvial fan deposits with scattered outcrops of the Jurassic – Early Cretaceous marine/continental sediments and Cretaceous volcanic units. The Precordillera is composed by some of the oldest rocks in the region that correspond to stratified volcanic and sedimentary sequences of Paleozoic to Mesozoic age, intruded by Paleozoic to Triassic and Paleocene-Eocene plutonic rocks (Hervé et al., 1991). The Western Cordillera is composed mostly of Tertiary andesitic volcanic rocks (Marinovic and García, 1999; Cortes, 2000; SERNAGEOMIN, 2003). The major structural features in the area are the strike-slip Atacama Fault System (AFS), the Antofagasta-Calama Lineament (ACL) and the Domeyko Fault System (DFZ) (Fig. 1B).

2.2. Climatic and hydrologic setting

The Atacama Desert of northern Chile is the driest desert on Earth and makes up much of the hyperarid margin of western South America (Fig. 1B). The hyperarid core of the Atacama Desert receives less than 2 mm/yr precipitation (Figs. 1B and 2), and scattered rainfall events occur only once every decade (Houston and Hartley, 2003; McKay et al., 2003; Garreaud et al., 2010). The western margin of the Atacama Desert receives consistent moisture in the form of coastal fog or sea spray, at elevations between 300 and 1000 m a.s.l. (Rundel et al., 1991). Along the eastern margin of the Atacama Desert, at the base of the Andes (~2500 m a.s.l.), precipitation is >20 mm/yr, and grades to a semiarid desert between 2700 and 3000 m a.s.l. (Fig. 1B). Occasional precipitation events in the central Atacama Desert generally result from Pacific air masses that migrate northward from the westerly precipitation. On the other hand, precipitation in the eastern margin of the Atacama Desert is associated with the South American summer monsoon (roughly 80% of annual rainfall occurs during the austral summer), where air masses spill over the central Andes and generate precipitation at elevations above ~2800 m a.s.l. (Houston and Hartley, 2003), but do not cause rainfall in the central Atacama (Zhou and Lau, 1998; Rech et al., 2006). Therefore, the main source of precipitation in this region is the Atlantic Ocean and most of the rain falls between December and March (Garreaud and Aceituno, 2001).

The extreme lack of precipitation is a feature that has remained stable over millions of years because of major coupled atmospheric and tectonic feedbacks (Rech et al., 2006). However, short-lived times of increased precipitation

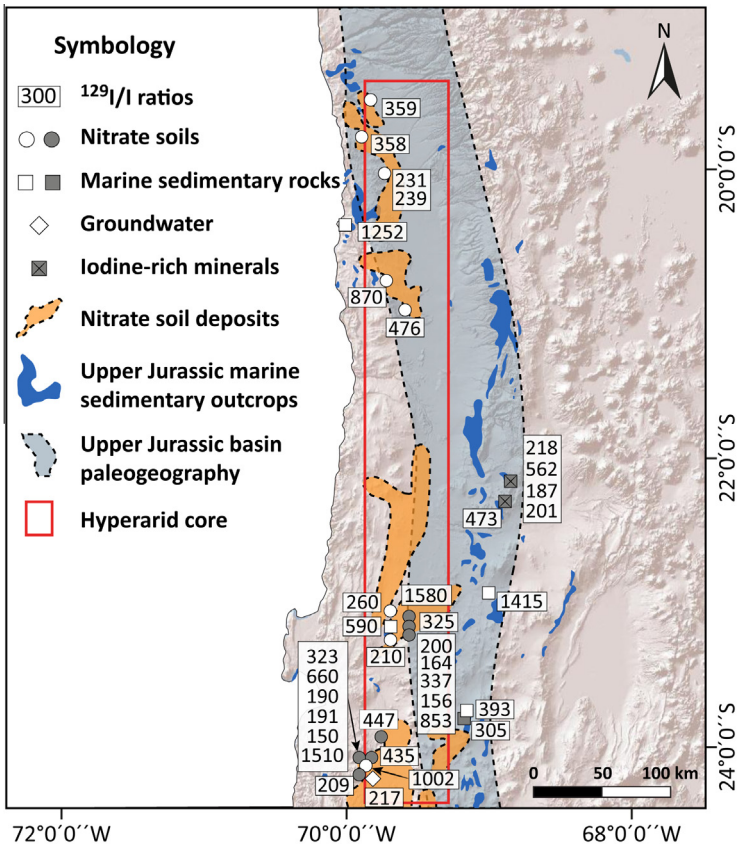

Fig. 2. Nitrate-rich soils in northern Chile and iodine isotopic ratios (^{129}I/I) distribution. Data points in gray correspond to results of other authors listed in Table 1.

exist in paleohydrological and pedological records (*e.g.*, late Quaternary, Betancourt et al., 2000; Ewing et al., 2006; Nester et al., 2007; Amundson et al., 2012).

Groundwater resources in the Atacama Desert are frequently stored in aquifers that are part of sedimentary sequences that were deposited during the Neogene and the Quaternary (*e.g.*, alluvial fan deposits), and have thicknesses of up to 900 m (Magaritz et al., 1990). Although there is limited hydrologic information in the south portion of the studied area (Antofagasta region), several investigations have studied the groundwater system to the north, where the main aquifers are located in the Pampa del Tamarugal (19° 30′–22°S), corresponding to a terminal basin of an endorheic drainage system (*e.g.*, Magaritz et al., 1990; Aravena, 1995; Gayó et al., 2012; Dorsaz et al., 2013). Isotopic, chemical and geological evidence support the hypothesis that a regional primary inflow to the aquifers in the hyperarid Atacama Desert occurs via groundwater associated with recharge areas located in the higher part of the Andes region (Magaritz et al., 1990; Aravena, 1995; Aravena et al., 1999). The most important recharge areas are located along the Western Cordillera and Sierra Moreno (Nester et al., 2007; Gayó et al., 2012). The recharge of the aquifers is strongly related to annual atmospheric conditions and the high topography of the Andes where annual rainfall increases from <10 mm/yr below 2000 m to 120 mm/yr at 4000 m elevation (Houston, 2002, 2006). Thus, precipitation over the High Andes generates surface water runoff and infiltration to aquifers, where discharge occurs as fracture flow through the volcanic units situated at the foothills of the Andes and in the Atacama Desert along the Central Depression (Magaritz et al., 1990).

The hydrologic environment in Atacama has exerted strong controls on the different types of sedimentary facies deposited. In the eastern canyons, alluvial fan deposits triggered by mass wasting due to the rare storms at high elevations are dominant (Houston, 2002, 2006). On the other hand, the regional groundwater flow goes from northeast to southwest feeding aquifers in the western part of the Central Depression. Here, the water table nearly intersects with the land surface allowing the generation of salt lakes or *salars* (Magaritz et al., 1990; Aravena et al., 1999).

Shallow aquifers and desert oases in the hyperarid zone have been known since pre-Colombian times, and were used by the communities surrounding nitrate mines over a century ago (Latorre et al., 2013). Despite the documented presence of the near-surface water table, the influence of groundwater on the accumulation of iodine and other components in the *caliche* deposits has often been ignored in previous studies. Currently, the water table levels in the Central Depression vary from near-surface in *salars* and wetlands (Rech et al., 2002) to 33–55 m (below surface) at the Pampa del Tamarugal (Leybourne and Cameron,

2006a). Other studies set the water table level at 30–90 m (below surface) near the Spence copper mine in the Central Depression (Leybourne and Cameron, 2006b) and 27 m (below surface) near the Salar de Imilac in Precordillera (Quade et al., 2008).

2.3. Iodine-rich nitrate soils and supergene copper deposits

The Atacama Desert is the premier source of natural iodine, which is highly concentrated in the nitrate-rich "saltpeter" soils or "caliche" deposits located between 19°S and 26°S (Fig. 2). These deposits are unique due to their mineralogical features and extension, and are composed of a complex mixture of nitrates (~7–15% NO_3), iodates, perchlorates, chromates and even borates (Ericksen, 1981; Chong, 1994). They are significantly enriched in iodine, with concentrations in excess of 500 ppm. Virtually all the iodine in the nitrates occurs as iodate minerals such as lautarite ($Ca(IO_3)_2$), fuenzalidite ($K_6(Na,K)_4Na_6Mg_{10}(SO_4)_{12}(IO_3)_{12}\cdot 12H_2O$) and hectorfloresite ($Na_9(IO_3)(SO_4)_4$) (Pueyo et al., 1998).

This almost continuous belt is only interrupted by *salars* (*e.g.*, Salar Grande and Salar de Llamara) and the Loa River. The iodine-rich nitrate deposits have a longitudinal extension that vary from a few kilometers to up to 30 km wide, and have been geographically separated in two distinctive domains in the Tarapacá and Antofagasta regions (Fig. 1A). Five historic districts are recognized from north to south: Tarapacá, Tocopilla, Baquedano, Aguas Blancas and Taltal. The nitrate deposits occur within alluvial fans cementing gravels, and also interstratified as vetiform and lenticular bodies (Ewing et al., 2006, 2007). Neogene alluvial fans along the eastern margin of Coastal Cordillera host large amounts of nitrates in a narrow, NS-trending, ~700 km long belt with an average altitude of ~1000 m a.s.l (Fig. 2). Typically, nitrate rich-soils cover the landscape and their maximum concentrations are found near the *salars*, also exhibiting east–west variations in their chemistry that are a function of the distance from marine aerosol sources (Rech et al., 2003; Ewing et al., 2006).

Nitrate soils vary between 3 and 13 m in thickness and consist of several horizons (Ericksen, 1981): (i) *chusca*: surface horizon (~30 cm) of powdery gypsum and anhydrite; (ii) *costra*: thick horizon below the *chusca* that ranges between ~50 cm and 2 m, and is composed of cemented gypsum and anhydrite; (iii) *caliche*: corresponds to a firmly-cemented horizon below the *costra* that varies from 1 to 5 m in thickness, and contains nitrate and other soluble salts; (iv) *conjelo*: is a horizon up to 2 m thick of salt-cemented regolith; and (v) *coba*: a loose, unconsolidated soil. A representative iodine-rich nitrate soil profile from the Aguas Blancas mine is shown in Fig. 5.

Several theories about the origin of nitrate deposits have been proposed since the 19th century. These hypotheses have pointed to biologic sources (Forbes, 1861; Noellner, 1867; Penrose, 1910; Gale, 1912; Brüggen, 1938), atmospheric/meteoric factors (Pissis, 1878; Singewald and Miller, 1916; Wetzel, 1924; Mueller, 1960; Ericksen, 1983; Böhlke et al., 1997; Michalski et al., 2004; Ewing et al., 2006, 2007, 2008), and volcanic inputs (Ericksen, 1961; Fiesta, 1966; Oyarzún and Oyarzún, 2007), to name a few. Even though the debate about the origin of nitrate deposits is still open, recent studies show robust evidence toward a multi-source origin for the principal components of nitrate deposits. These include dominant atmospheric sources, such as marine aerosol, for the nitrate, sulfate and calcium components (Böhlke et al., 1997; Rech et al., 2003; Michalski et al., 2004; Ewing et al., 2006, 2007, 2008). The oxygen-17 data in perchlorate present in the Atacama nitrate soils are also consistent with a natural atmospheric origin for this component (Bao and Gu, 2004). Most recently, a groundwater source model has been proposed to explain the presence of chromate and iodate components in the nitrates (Pérez-Fodich et al., 2014).

Apart from nitrate deposits, iodine mineral occurrences in Atacama have been documented in the supergene zones of porphyry and Manto-type copper deposits (Fig. 1B). The copper-iodide marshite (CuI) and other copper-iodate minerals such as salesite [$Cu(IO_3)(OH)$] and bellingerite [$Cu_3(IO_3)_6)\cdot 2H_2O$] were reported to occur in the oxide zone of the giant Chuquicamata Cu deposit (Jarrell, 1939, 1944), while the silver iodide iodargyrite (AgI) was documented more recently at the Mantos de la Luna Cu-Ag deposit (Reich et al., 2009a). Geochemical surveys have also shown high iodine concentrations in soils above giant Cu deposits (*e.g.,* Spence, Chimborazo; Cameron et al., 2010 and Kelley et al., 2003; Fig. 1B), and fossil soil anomalies have been reported at the Pampa del Tamarugal (Leybourne and Cameron, 2006a). Almost all of these geochemical anomalies occur above fracture zones in the gravels that can be correlated to deeper structural features of the hypogene deposits (Cameron et al., 2002). At the Spence porphyry Cu deposit, Leybourne and Cameron (2006b) have reported high iodine concentrations (>65 ppm) along with high Cu concentrations (2 ppm) in saline groundwaters. Thus, recent studies have related the occurrence of Cu-(halogen) soil anomalies to deep-sourced saline groundwaters that have been pumped to the surface along active faults and/or fractures during seismic events (Cameron et al., 2002, 2007, 2008; Reich et al., 2008, 2009b; Leybourne et al., 2013).

2.4. Iodine geochemistry and the ^{129}I isotopic system

In oxidized form (as iodate or I_2 molecules) iodine has the most biophilic nature among the halogens and is commonly associated with organic material (Elderfield and Truesdale, 1980; Wong, 1991). As a member of the halogen group, iodine shares characteristics with chlorine (Cl) and bromine (Br), but iodine has the largest ionic radius of the three elements and is much less frequently incorporated into minerals. Thus, iodine in reduced form remains in the aqueous phase much longer than chlorine, the least biophilic element of these three. While the largest reservoir of chlorine in the Earth's surface is seawater, iodine is concentrated in marine sediments where the total amount of iodine reaches up to 5.90×10^{12} tonnes, corresponding to ~70% of the total iodine inventory in the Earth's crust (Muramatsu and Wedepohl, 1998). Due to its biophilic behavior, iodine in marine particulate organic matter varies

from 200 to 1300 ppm while seawater contains approximately 0.05 ppm iodine (Wong, 1991; Muramatsu and Wedepohl, 1998).

Iodine has one stable isotope (^{127}I), and a long-lived radioisotope (^{129}I) with a half-life of 15.7 Ma. In nature, ^{129}I is mainly produced by cosmic ray-induced spallation of Xe isotopes in the atmosphere (cosmogenic component) and by spontaneous fission of ^{238}U in crustal rocks (fissiogenic component). Both production pathways contribute similar amounts of natural ^{129}I to surface reservoirs (Fabryka-Martin et al., 1985). Since there is only one stable isotope of iodine (^{127}I) and the radiogenic isotope ^{129}I is present in very small amounts, ^{129}I/I (^{129}I over total iodine) is for all practical purposes identical to ^{129}I/^{127}I. Due to the long residence time of iodine in the oceans (300,000 yr, Broecker and Peng, 1982) and the fact that iodine moves quickly through most surface reservoirs, natural iodine is in isotopic equilibrium in all surface reservoirs, with an initial ^{129}I-to-stable ^{127}I isotopic ratio (^{129}I/I) of $(1500 \pm 150) \times 10^{-15}$ at·at^{-1} (Fehn et al., 2007a). This ratio is independent of latitudinal variations in the production of cosmogenic ^{129}I and is considered as the starting value for ^{129}I calculations. The equilibrium in surface reservoirs has been disturbed since ~1945 by the addition of anthropogenic ^{129}I from nuclear weapons tests and fuel reprocessing which has increased the ^{129}I/I ratio of surficial reservoirs by several orders of magnitude (Snyder and Fehn, 2004). Thus, in most cases the anthropogenic ^{129}I signal can be detected because of the large difference between anthropogenic and natural values (Fehn et al., 2007a). Although this signal is present in all surface reservoirs which are in rapid exchange with the oceans, anthropogenic ^{129}I is not affecting marine sediments, deep fluids and aquifers with ages >60 yr.

While the initial ^{129}I/I ratio in surface reservoirs is $\sim 1500 \times 10^{-15}$, different values have been reported in fore-arc, volcanic and deep crustal fluids. The ^{129}I/I ratios in fore-arc fluids are significantly lower than surficial reservoirs, ranging between ~100 and 500×10^{-15}. These fluids contain "old" cosmogenic iodine that has been derived from organic material, and are hosted in marine sequences that are substantially older (Fehn et al., 2004, 2007a; Lu et al., 2011). In contrast, volcanic fluids from active continental margins have higher ratios, with values that range between 700 and 1000×10^{-15} (*e.g.*, Snyder et al., 2002). These values reflect the age of the subducted slab, indicating a "young", slab-derived marine sediment source component for iodine in volcanic fluids (Snyder and Fehn, 2002; Snyder et al., 2003). When iodine is separated from its original source (*e.g.*, marine sediment source), the isotopic equilibrium is broken and the cosmogenic signal starts to decrease as a function of time until secular equilibrium with the fissiogenic (*in situ*) signal is reached (Fehn et al., 2007a). Additionally, deep crustal fluids can show high ^{129}I/I ratios ($>2000 \times 10^{-15}$) due to accumulation of ^{129}I from rock sources that are anomalously enriched in uranium (*e.g.*, Andrews et al., 1989; Bottomley et al., 2002; Snyder et al., 2003; Fehn and Snyder, 2005).

The iodine isotopic system has received increasing attention because it covers an age range of wide applicability including, for example: (1) tracing groundwater and geothermal fluid sources (*e.g.*, Fabryka-Martin et al., 1991; Frohlich et al., 1991; Fehn et al., 2000), (2) unraveling the origin and transport history of deep crustal fluids (*e.g.*, Fehn and Snyder, 2005), (3) dating oil field brines and coalbed methane (*e.g.*, Fehn et al., 1990; Snyder and Fabryka-Martin, 2007) and (4) investigating sediment recycling in subduction zones (Martin et al., 1993; Lu et al., 2008), where iodine source compartments include subducting marine sediments (*e.g.*, Snyder and Fehn, 2002), organic-rich formations in the overlying plate (*e.g.*, Fehn and Snyder, 2003) and, to a lesser extent, a serpentinized sub-arc mantle wedge (*e.g.*, Snyder et al., 2005). These different applications are possible due to the existence of the two natural modes of iodine production (*i.e.,* cosmogenic and fissiogenic). Since the cosmogenic signal predominates in fluids related to organic material, the measured ^{129}I/I ratios allows to determine the time of separation from surficial reservoirs (Moran et al., 1995; Snyder et al., 2003). Otherwise, the fissiogenic signal is more important in fluids hosted in U-rich rocks in the crust, where the ^{129}I/I ratios have been used to calculate the age and residence time of fluids in deep formations (Fabryka-Martin et al., 1989; Fehn et al., 1992; Bottomley et al., 2002).

3. SAMPLES AND METHODS

Rock, nitrate soils and water samples were collected in the study area (~100,000 km^2), including the Coastal Range, Central Depression, Precordillera and Western Cordillera in northern Chile (Fig. 1B). These selected samples are representative of different reservoirs in the Atacama region, and include nitrate deposits from the Tarapacá and Antofagasta districts in the Central Depression (Tarapacá, Baquedano and Aguas Blancas districts), Jurassic marine sedimentary rocks outcropping in the Central Depression and Precordillera, and geothermal fluids from the Puchuldiza and El Tatio geothermal fields in the High Andes (Figs. 1 and 2). In addition, groundwater samples were collected from wells in the Central Depression and below nitrate deposits, and from salt lakes or "*salars*" in the Precordillera. Meteoric water samples were collected from surface streams in the Central Depression, Precordillera and Western Cordillera, including the Loa, San Pedro and Pufica rivers. Rainwater samples were collected during the 2010–2012 period. Custom-made stations were placed in selected areas in the Western Cordillera and Central Depression, and samples were retrieved after rainfall events. Light paraffin oil was placed at the bottom of the collector to seal the sample and prevent evaporation. The thickness of the paraffin oil layer floating on the water was ~0.5 cm. Finally, seawater samples were taken along the coast, near the cities of Iquique and Antofagasta.

For water samples, temperature, conductivity and pH were measured *in situ* (Table 2) and 250 ml were collected and filtered (0.45 μm Millipore filter) for chemical analysis. Previous to iodine extraction for Accelerator Mass Spectrometry (AMS) ^{129}I/I isotopic determinations, all water, rock and soil samples were analyzed for iodine concentrations using inductively-coupled plasma mass

spectrometry (ICP-MS) at Rice University in Houston and Gakushuin University in Tokyo. Water samples were diluted 200–5000 times and tetramethyl ammonium hydroxide (1%), and 100 ppm Na_2SO_3 were added to avoid loss of iodine from the solution prior to the ICP-MS determination. For rocks and soils, approximately 50 g of sample material was powdered and combined with 100 ml of purified 18 MΩ water and placed in 250 ml high-density polyethylene container. In order to enhance iodate dissolution, samples were agitated during 8 h and centrifuged for 30 min at 1000 rpm. Iodine was extracted from water and solid samples following established methods, *i.e.*, extraction into chloroform or carbon tetrachloride followed by back extraction using sodium bisulfite or hydroxylamine hydrochloride (Fehn et al., 1992). Finally, approximately 1 mg of iodine was precipitated as silver iodide (AgI) targets for AMS isotopic determinations. The AMS measurements were performed at Prime Lab, Purdue University (Indiana), following established procedures (Sharma et al., 2000). The analytical error (1σ) for each analyzed sample is included in Table 1. Due to the small size of the targets, ratios generally have errors between 5% and 25%. Because the ^{129}I abundance depends on the total amount of iodine in samples, values are expressed as $^{129}I/I$ ratios. The theoretical AMS detection limit is on the order of 2×10^{-15} ^{129}I atoms per total I atoms, estimated based on counting statistics and measurement times. However, the practical detection limit is somewhat higher because of the lack of suitable blank materials with ratios below $\sim 20 \times 10^{-15}$ (Fehn et al., 2007a).

4. RESULTS

4.1. Iodine concentrations

Iodine concentrations of nitrate soils and rock samples from the Atacama Desert are listed in Table 1. The nitrate samples of the Tarapacá and Antofagasta districts contain the highest iodine concentrations of all reservoirs in the Atacama region, with a mean concentration of ~700 ppm, with maximum and minimum values of ~4000 ppm and 2 ppm, respectively (Table 1). Soils above the Spence and Mina Sur copper deposits in the Central Depression and Precordillera show iodine concentrations in excess of 100 ppm above fracture zones crosscutting supergene copper mineralization (Cameron et al., 2010; Reich et al., 2013). Mesozoic shales and limestones are also enriched in iodine, averaging ~50 ppm in the Antofagasta region (*i.e.*, Caracoles Group), with a maximum iodine concentration of ~130 ppm (Table 1). These values are significantly higher than Mesozoic sedimentary marine rocks (shales and calcareous siltstones) in the northern portion of the studied area (Tarapacá, iodine concentrations <1 ppm). Additionally, iodine concentrations above crustal averages are found in selected continental sedimentary rocks, siliceous sinter deposits and lacustrine evaporite samples in the study area, with iodine concentrations varying between ~1 and 6 ppm (Table 1).

Iodine concentrations of water samples are reported in Table 2. The highest concentrations of iodine were measured in groundwater below nitrate deposits with values between 0.5 and 48 μM, averaging ~12 μM, and the highest concentrations are found in the Antofagasta region (sample A1; Table 2). These high iodine concentrations are followed by water samples from the Puchuldiza (~21 μM) and El Tatio (~7 μM) geothermal springs in the Western Cordillera. Spring waters from the Precordillera present values between ~1 and 12 μM (average of ~5 μM), and waters from salt lakes ("salars") have concentrations from 0.25 to 8 μM (average of ~3 μM). Finally, the lowest iodine contents were measured in seawater (near Antofagasta), surface water and rain water with an average of ~0.7 μM, although surficial (river) water from the Western Cordillera present slightly higher values.

4.2. $^{129}I/I$ isotopic ratios

The $^{129}I/I$ ratios (at 1σ error) of soil/rock and water samples are listed in Tables 1 and 2, and sample distribution is shown in Fig. 2. The results for each reservoir are plotted schematically in Fig. 3. The $^{129}I/I$ ratios of the high-iodine nitrates from the Tarapacá district in the northern part of the study area are low and range from 230 to $\sim 870 \times 10^{-15}$, while the $^{129}I/I$ ratios of nitrate soils in the Antofagasta region, show a larger dispersion and range from ~150 to $\sim 1500 \times 10^{-15}$ (Pérez-Fodich et al., 2014). The iodine isotopic ratios for Mesozoic marine sedimentary rocks could only be obtained for two shales and one calcareous sandstone (Antofagasta samples), and vary from ~300 to $\sim 600 \times 10^{-15}$. Because of the relatively low concentrations of iodine in the water samples, an isotope ratio could only be determined in one groundwater sample. This sample from the Central Depression below nitrate soils in the Aguas Blancas district yielded a $^{129}I/I$ ratio of 217×10^{-15} (Table 2; Figs. 2 and 3).

5. DISCUSSION

5.1. Distribution of iodine in Atacama

Iodine concentrations in nitrate soils, soils above Cu deposits and selected rock samples from the Atacama region (Table 1) are considerably higher than the average crustal value of ~0.12 ppm (Muramatsu and Wedepohl, 1998). Iodine concentrations in the studied samples are plotted in Fig. 4 and compared to natural iodine reservoirs (Fehn, 2012). Fig. 4 shows that selected soils and Mesozoic marine sedimentary rocks from Atacama are strongly enriched in iodine compared to most natural reservoirs (rocks and organic-rich sediments). Water samples (groundwater, geothermal waters and spring waters) also show elevated iodine concentrations, within the range of pore waters in marine formations and volcanic fluids. In the case of freshwaters from Atacama, iodine concentrations are one order of magnitude higher than the average in continental meteoric waters. Concerning iodine distribution in soils, rocks and waters from Atacama region, concentrations reach maximum values in the nitrate belt of Antofagasta (1000's ppm range; Table 1), although high iodine values in soils and groundwater are distributed over

Table 1
Analytical results of iodine concentrations and $^{129}I/I$ ratios in soils, sediments and rocks.

Site	Sample	Type	Location (UTM)		Elevation (masl)	Soil depth (m)	I concentration (ppm)	$^{129}I/I$ (10^{-15} at·at^{-1})	1σ (10^{-15}at·at^{-1})	^{129}I concentration (10^{7} at/kg)
			Latitude (°S)	Longitude (°W)						
Tarapacá										
T3	T3A-A	Nitrate soil	21° 2′ 25″	69° 37′ 30″	889	0.50	2.00	ND		
	T3E-A	Nitrate soil			889	0.60	28.57	476	30	6.45
	T3C-A	Nitrate soil			889	0.80	4.78	LCV		
	T3D-A	Nitrate soil			889	1.05	38.50	ND		
T4	T4A-A	Nitrate soil	20° 50′ 15″	69° 43′ 15″	960	0.25	24.81	ND		
	T4B-A	Nitrate soil			960	0.30	17.39	870	112	7.18
T6	T6B-A	Sandstone	20° 15′ 43″	70° 02′ 04″	802	–	0.74	AV		
	T6C-A	Shale			802	–	0.39	ND		
T8	T8B-A	Nitrate soil	19° 52′ 20″	69° 49′ 20″	1176	0.30	46.45	LCV		
	T8A-A	Nitrate soil			1176	0.80	74.58	359	46	12.71
T9	T9A-A	Nitrate soil	20° 03′ 04″	69° 45′ 58″	1114	0.20	61.70	358	83	10.48
T10	T10B-A	Nitrate soil	20° 02′ 48″	69° 45′ 53″	1123	0.40	120.75	239	39	13.70
	T10A-A	Nitrate soil			1123	0.50	839.94	231	33	92.08
T12	T12A-A	Shale	20° 55′ 41″	69° 03′ 37″	2263	–	0.60	LCV		
T16	T16A-A	Siltstone	20° 55′ 41″	69° 03′ 37″	2263	–	0.75	ND		
Antofagasta										
M1	M1G-A*	Nitrate soil	24° 09′ 25″	69° 51′ 40″	1048	0.10	101.98	323	115	15.63
	M1E-A*	Nitrate soil			1048	0.40	817.90	660	236	256.17
	M1D-A*	Nitrate soil			1048	0.70	2439.27	190	15	219.94
	M1F-A*	Nitrate soil			1048	1.10	1003.46	191	14	90.95
	M1C-A*	Nitrate soil			1048	1.40	912.36	150	10	64.95
	M1B-A	Nitrate soil			1048	1.70	24.70	ND		
	M1A-A*	Nitrate soil			1048	2.15	59.60	1510	371	42.71
M2	M2A-A*	Nitrate soil	24° 09′ 25″	69° 51′ 40″	1048	1.30	237.11	435	74	48.95
M3	M3A-A	Nitrate soil	24° 09′ 25″	69° 51′ 40″	1048	1.10	168.75	1002	460	80.24
M4	M4A-A	Nitrate soil	24° 09′ 14″	69° 52′ 27″	1049	0.80	96.37	LCV		
M5	M5B-A*	Nitrate soil	24° 10′ 01″	69° 51′ 12″	1068	1.05	152.39	209	49	15.11
M6	M6B-A*	Nitrate soil	24° 08′ 39″	69° 53′ 54″	1038	1.30	846.67	447	99	179.60
M7	M7B-A*	Nitrate soil	23° 12′ 28″	69° 41′ 32″	1274	0.70	75.76	1580	244	56.80
M8	M8A-A	Nitrate soil	23° 11′ 58″	69° 41′ 13″	1299	0.30	4.39	ND		
	M8B-A*	Nitrate soil			1299	1.10	3978.63	325	79	613.63
M9	M9B-A*	Nitrate soil	23° 12′ 05″	69° 41′ 24″	1295	0.40	475.87	200	31	45.17
	M9E-A*	Nitrate soil			1295	1.05	261.05	164	18	20.32
	M9D-A*	Nitrate soil			1295	1.20	519.44	338	130	83.32
	M9A-A*	Nitrate soil			1295	1.35	476.67	156	13	35.29
	M9C-A*	Nitrate soil			1295	1.80	92.35	853	229	37.38
M10	M10A-A	Sinter	22° 19′ 48″	68° 00′ 36″	4281	0.00	6.08	ND		
M11	M11A-A	Evaporite rock	23° 03′ 54″	68° 12′ 52″	2337	0.00	32.00	1415	72	21.49
M12	M12A-A	Nitrate soil	23° 11′ 58″	69° 41′ 13″	1305	1.10	824.51	210	30	82.17
M13	M13A-A	Shale	23° 11′ 58″	69° 41′ 13″	1305	–	37.58	590	60	10.52

(*continued on next page*)

Table 1 (*continued*)

Site	Sample	Type	Location (UTM)		Elevation (masl)	Soil depth (m)	I concentration (ppm)	$^{129}I/I$ (10^{-15} at·at^{-1})	1σ (10^{-15}at·at^{-1})	^{129}I concentration (10^7 at/kg)
			Latitude (°S)	Longitude (°W)						
M14	M14A-A	Nitrate soil	23° 11′ 11″	69° 39′ 22″	1336	0.50	896.78	260	50	110.65
MC	MC3A-A	Calcareous siltstone	22° 55′ 52″	68° 58′ 19″	2494	–	9.08	ND		
	MC3B-A*	Shale			2494	–	128.46	393	74	23.96
	MC3D-A	Calcareous sandstone			2494	–	2.30	305	76	0.33
	MC4A-A	Shale			2494	–	3.64	ND		
	MC5A-A	Calcareous sandstone			2494	–	4.15	ND		
CH	C103579**	Marshite	22° 17′ 12″	68° 54′ 03″	2260	–	ND	218	72	
	105768**	Marshite			2260	–	ND	562	77	
	Atac-Ch**	Marshite			2260	–	1704.09	187	17	151.22
	Mshxx-B**	Marshite			2260	–	11415.66	207	14	1121.40
MM	EMC107**	Iodine-rich soil	22° 23′ 56″	68° 55′ 28″	2343	ND	ND	473	75	

ND: Not determined; LCV: Low current values.
* $^{129}I/I$ ratios and iodine concentration data from Pérez-Fodich et al. (2014).
** $^{129}I/I$ ratios from Reich et al. (2013), concentration data were determined in this study.

a much wider area (Fig. 2). No other significant relations are observed between latitude or longitude and iodine concentrations, although soils and groundwater in the Central Depression generally contain higher iodine concentrations than in the other morphostructural units shown in Fig. 1A.

In general, the iodine isotopic ratio of soils, rocks and waters show no significant longitudinal or latitudinal variations. However, nitrate deposits are characterized by variations in $^{129}I/I$ ratios and iodine concentrations along soil profiles. In order to better understand how iodine is distributed in these soils, we studied a depth profile of a representative iodine-rich nitrate soil hosted in an alluvial fan deposit in the Aguas Blancas iodine mine (site M1, Fig. 1B). Fig. 5 shows the iodine concentrations and isotopic ratios for each sample in a profile of 2.3 m thickness. Iodine concentrations show a sharp increase from the top layer (102 ppm in *chusca*; Fig. 5) to the nitrate-rich core of the soil profile. Within this portion (~1.3–1.8 m), iodine is significantly high and ranges from 912 to 2439 ppm in the *conjelo* and *caliche*, respectively (Fig. 5). Iodine concentrations decrease below the *caliche* by almost two orders of magnitude to 25–60 ppm in *coba*. The highest iodine concentrations observed in the soil profile are closely related with the highly cemented horizon, *i.e.*, the *caliche* layer that contain low detrital components, while the lowest concentrations are associated with the unconsolidated regolith (*coba*) below the *caliche* horizon.

The highest iodine concentrations along the soil profile strongly correlate with the lowest $^{129}I/I$ ratios (between 150 and 191×10^{-15}) observed in the more cemented horizons, *i.e.*, the *caliche* and *conjelo*. In the upper non-consolidated soil horizons (*chusca*), the isotopic ratios are higher (323 and 660×10^{-15}) but still substantially lower than the pre-anthropogenic ratio of 1500×10^{-15}, typical of surface (meteoric) reservoirs. It is noteworthy that the highest $^{129}I/I$ ratio (1510×10^{-15}), located at the bottom of the soil profile, is associated with the lowest iodine concentrations (Fig. 5).

The observation that samples with lower iodine concentrations have higher isotopic ratios points to the input of pre-anthropogenic meteoric water, because this relict "surficial" signal is more easily detectable in samples in which the initial concentrations of stable iodine are low. Based on these observations, we suggest that iodine distribution and isotopic ratio variations in nitrate soils may be related to changes in climate such as increased surface precipitation (meteoric water addition) and/or inputs of groundwater with "older" signatures. Previous studies have suggested that vertical variation in nitrate soil chemistry in the Atacama Desert may be related to events of downward water movement (Ewing et al., 2006, 2008). Based on nitrate and chloride distribution in soils from Atacama, in the southern boundary of our study area, Ewing et al. (2006) related the increased concentrations within a ~1.5 m layer to rare rainfall events on a centennial to millennial scale. This interpretation is consistent with our new iodine data, since recent downward flow in nitrate soils would shift the originally low $^{129}I/I$ ratios of *caliche* to higher, more meteoric values by isotopic mixing within

Table 2
Analytical results of iodine concentrations in water samples.

Sample	Morphostructural unit	Type	Location		pH	T° (°C)	EC (μS/cm)	I concentration (μM)
			Latitude (°S)	Longitude (°W)				
Tarapaca								
TA1	Tarapaca Coast	Seawater	20° 39′ 36″	70° 11′ 06″	8.1	17.2	ND	0.37
TA2	Central Depression	River	21° 37′ 31″	69° 33′ 17″	7.7	17.9	5870	1.56
TA3	Central Depression	Groundwater	20° 50′ 21″	69° 42′ 49″	ND	ND	ND	22.29
TA4	Central Depression	Groundwater	19° 53′ 05″	69° 51′ 54″	7.5	31.7	2780	7.25
TA5	Western Cordillera	Salt lake	20° 18′ 23″	68° 52′ 33″	6.1	14.5	8600	7.99
TA6	Western Cordillera	Salt lake	20° 18′ 23″	68° 52′ 33″	ND	ND	ND	1.00
TA7	Western Cordillera	Spring	20° 18′ 32″	68° 52′ 21″	6.7	15.6	940	0.35
TA8	Precordillera	Spring	20° 57′ 50″	69° 10′ 23″	7.3	22.1	2290	3.85
TA9	Precordillera	Spring	20° 57′ 50″	69° 10′ 23″	7.4	22.1	2240	10.36
TA10	Precordillera	Spring	20° 57′ 50″	69° 10′ 23″	7.3	21.8	2250	12.00
TA11	Precordillera	Spring	20° 55′ 45″	69° 05′ 48″	8.1	14.4	1950	3.76
TA12	Western Cordillera	Geothermal	19° 24′ 38″	68° 58′ 17″	8.4	19.2	3800	18.35
TA13	Western Cordillera	Geothermal	19° 24′ 51″	68° 57′ 45″	6.8	50.0	4300	15.23
TA14	Western Cordillera	Geothermal	19° 24′ 44″	68° 57′ 33″	8.0	84.0	4600	26.24
TA15	Western Cordillera	River	19° 40′ 49″	69° 10′ 53″	7.9	16.5	390	0.36
TA16	Western Cordillera	Geothermal	19° 40′ 59″	69° 10′ 36″	8.4	40.0	450	0.54
TA17	Precordillera	Spring	20° 29′ 14″	69° 19′ 06″	8.2	30.3	170	1.25
TA18	Precordillera	Spring	20° 29′ 14″	69° 19′ 06″	8.5	10.0	ND	2.29
Antofagasta								
A1*	Central Depression	Groundwater	24° 10′ 31″	69° 52′ 07″	7.2	22.8	1570	48.12
A2	Central Depression	Groundwater	24° 10′ 38″	69° 52′ 06″	6.9	18.4	1010	1.17
A3	Central Depression	Groundwater	24° 03′ 29″	69° 49′ 31″	7.7	22.7	3570	4.26
A4	Antofagasta Coast	Seawater	23° 28′ 10″	70° 30′ 46″	7.8	16.8	ND	0.40
A5	Antofagasta Coast	Seawater	22° 28′ 35″	68° 54′ 51″	7.9	16.5	ND	0.44
A6	Central Depression	River	22° 55′ 20″	68° 09′ 59″	7.8	15.3	7235	0.93
A7	Central Depression	Groundwater	22° 53′ 25″	68° 12′ 50″	6.4	28.6	3670	2.64
A8	Central Depression	River	23° 03′ 54″	68° 12′ 52″	7.3	22.4	5510	0.25
A9	Atacama Basin	Salt lake	23° 03′ 32″	68° 12′ 49″	7.8	16.0	ND	6.18
A10	Atacama Basin	Groundwater	23° 03′ 32″	68° 12′ 49″	ND	ND	ND	0.46
A12	Atacama Basin	Salt lake	23° 07′ 40″	68° 14′ 39″	7.0	23.5	ND	0.25
A13	Western Cordillera	Geothermal	22° 19′ 48″	68° 00′ 36″	6.8	81.0	ND	7.92
A14	Western Cordillera	Geothermal	22° 24′ 24″	68° 00′ 41″	6.4	85.5	ND	6.29
A15	Western Cordillera	Lake	22° 25′ 58″	68° 02′ 57″	7.7	16.9	1020	0.51
A16	Western Cordillera	Spring	22° 43′ 12″	68° 02′ 37″	ND	ND	ND	1.78
A17	Western Cordillera	River	22° 46′ 09″	68° 04′ 07″	8.4	11.0	2240	1.49
A18	Western Cordillera	Lake	22° 25′ 58″	68° 02′ 57″	7.7	13.9	1360	0.37
A19	Western Cordillera	River	22° 46′ 09″	68° 04′0 7″	8.8	20.2	2120	1.51
A20	Western Cordillera	Salt lake	23° 03′ 54″	68° 12′ 52″	8.2	19.7	ND	3.59
AM-02	Western Cordillera	Rainwater	22° 25′ 59″	68° 02′ 57″	7.7	ND	1180	0.29
AM-04	Central Depression	Rainwater	22° 42′ 06″	68° 26′ 44″	7.8	ND	1175	0.50

ND: Not determined.
* This sample yielded a $^{129}I/I$ ratio of 217 ± 18 and ^{129}I concentration of 0.63×10^7 at/L.

the less cemented horizons (*e.g.*, *chusca* and *coba*, Fig. 5). However, it is important to mention that a model that exclusively considers iodine contribution to nitrate soils from liquid or dry precipitation sources does not fully explain the lower isotopic values that correlate with the significantly high iodine concentrations in the *caliche* horizons. In order to assess the feasibility of this model, we estimated the time required to reach the current iodine concentration through both precipitation mechanisms. As a first approximation, we considered a mean iodine concentration and thicknesses of the *chusca*, *caliche*, *conjelo* and *coba* as shown in Fig. 5, and an average density of 1900 kg/m^3 (Ewing et al., 2006), obtaining a total iodine content of 4.4 kg/m^2. Assuming a steady state precipitation rate of 10 mm/yr and a meteoric iodine concentration of approximately 30 nmol/L (Gilfedder et al., 2008), it would take ~120 Myr to accumulate this amount of iodine through a cycle of precipitation and drying, clearly much longer than the period of hyperaridity in the region (at least 6 Ma and perhaps as long as 15 Ma; Alpers and Brimhall, 1988; Hartley and Chong, 2002).

Dry deposition is another possibility that has been used to explain the presence of iodine in nitrate soils. Using a molar ratio IO_3^-/NO_3^- of 0.0034 (or 0.0096 in weight; Grossling and Ericksen, 1971), and a total estimated deposition flux of 16.5 mg N m^2 yr^{-1} (Michalski et al.,

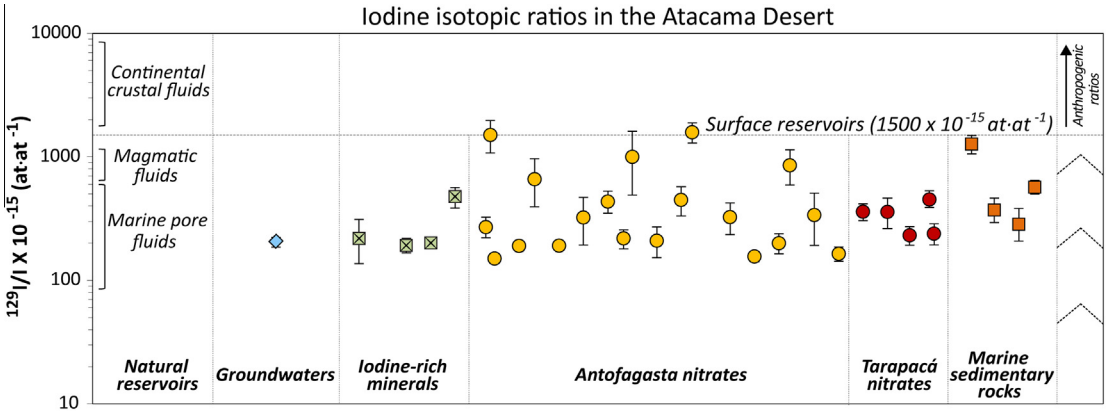

Fig. 3. Iodine isotopic ratios (^{129}I/I) of water, rock and soil samples from the Atacama Desert. Most of the ^{129}I/I ratios range between ~150 to 450 × 10^{-15} and all values are at or below 1500 × 10^{-15} (initial isotopic ratio of surface reservoirs; Fehn et al., 2007a). The Chuquicamata Cu deposit data are taken from Reich et al. (2013). Selected Antofagasta nitrate samples and one marine sedimentary rock data are taken from Pérez-Fodich et al. (2014). Detailed information about samples is presented in Table 1.

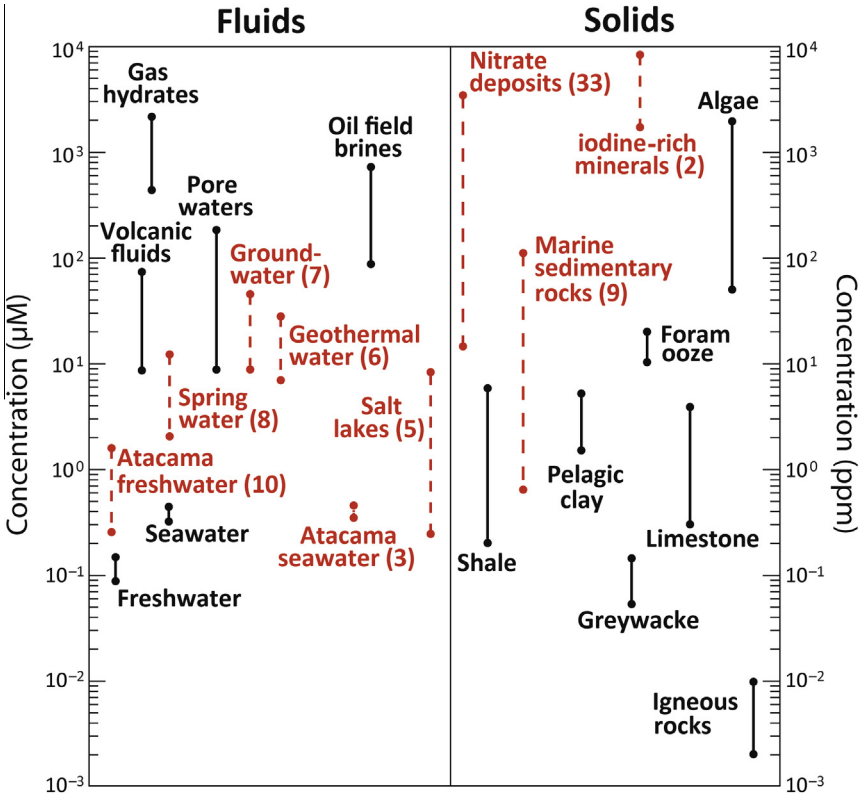

Fig. 4. Concentration ranges of iodine in rock, soils and water in the Atacama region (red segmented lines). The concentration ranges of fluids and solids in natural reservoirs are shown after Fehn (2012) (solid black lines). Numbers in parenthesis show the number of samples analyzed for each material. (For interpretation of the references to color in this figure legend, the reader is referred to the web version of this article.)

2004), the estimated time to reach the current iodine content of 4.4 kg/m^2 (and assuming 100% of retention) is ~26.5 Ma. This period of atmospheric deposition of iodine is more than twice the estimated age of nitrate deposits, which is related to the onset of hyper-arid conditions of the Atacama Desert. Even though mass balance calculations indicate that atmospheric deposition cannot explain the high contents of iodine and low isotopic ratios reported in the nitrates, we stress the importance of the atmospheric input for most of the other components of the nitrate soils. The atmospheric signature is indeed recorded in the nitrates, but it does not explain by itself the massive occurrence of iodine in Atacama. In the next sections we evaluate the participation of a deep and "old" organic source with

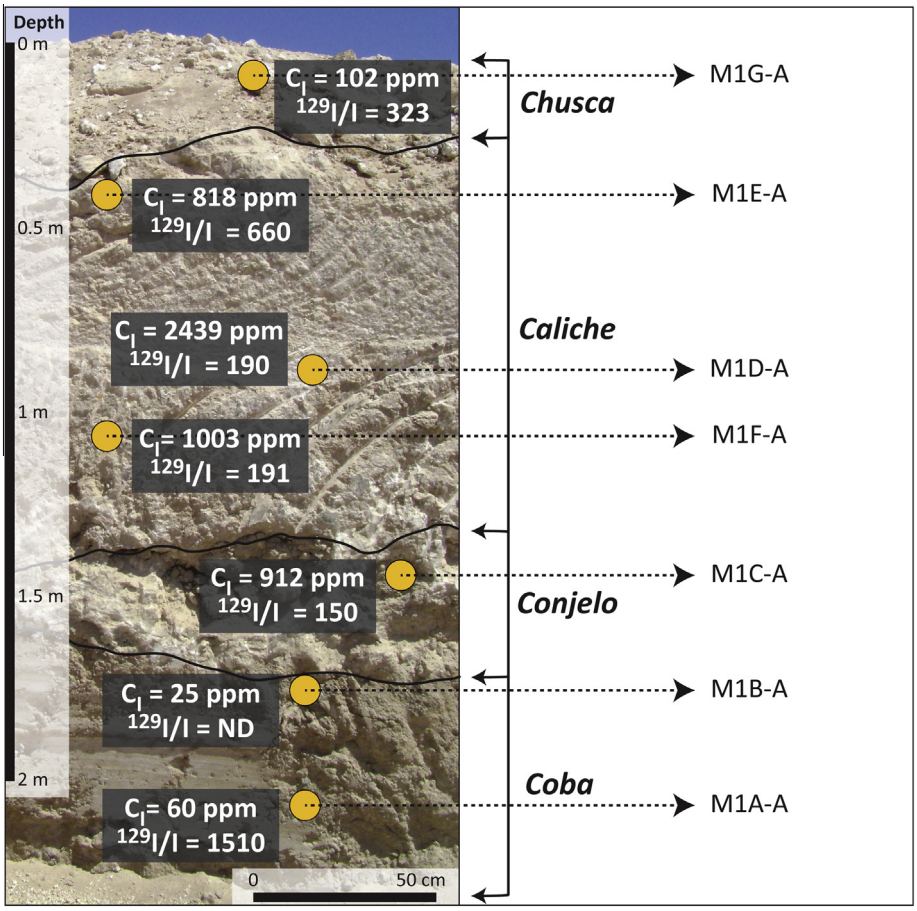

Fig. 5. Representative soil profile at the Aguas Blancas iodine mine near Antofagasta. Iodine concentrations (ppm) and isotopic ratios ($^{129}I/I$) of selected samples are shown in each soil horizon.

low $^{129}I/I$ ratios and high iodine concentrations as an additional source of iodine in the Atacama region.

5.2. Sources of iodine

Most of the Earth's surficial iodine resides in marine sediments along continental margins, intra and back-arc marine basins, and nearly 98.8% of the total atmospheric iodine is contributed by oceans due to air-sea exchange, where iodine is transferred from the oceans to the atmosphere and land (Muramatsu and Wedepohl, 1998; Snyder et al., 2010). For this reason and because of its high mobility, iodine is strongly depleted in continental environments. Thus, any model proposed to explain the anomalously high iodine concentrations in Atacama region requires a concentrated iodine source and/or concentration process. In both cases, a process that removes iodine from its original source to its final sink is necessary. Finally, and in order to preserve an originally "old" signature, strong iodine fixation and long-term preservation are needed.

Iodine enrichment in terrestrial environments can be related to the following sources: (i) Atmospheric "young" iodine derived from seawater, rivers, lakes and other surficial reservoirs, deposited by liquid, solid or dry (aerosol) precipitation. This source will present a pre-anthropogenic isotopic signal of $\sim 1500 \times 10^{-15}$ (initial ratio, Moran et al., 1998; Fehn et al., 2007a), or in certain cases higher ratios caused by anthropogenic iodine contamination (Schink et al., 1995; Rao and Fehn, 1999; Snyder and Fehn, 2004); (ii) "Old" cosmogenic iodine stored in rocks and weathered soils, in particular from marine sedimentary formations that have low ratios usually between 100 and 500×10^{-15} (Fehn et al., 2004, 2007a; Lu et al., 2011); (iii) Iodine from volcanic fluids that have variable ratios between 500 and 800×10^{-15} (Snyder and Fehn, 2002; Snyder et al., 2002).

Fig. 3 shows that the isotopic signature of iodine in most nitrate soils from Atacama, supergene Cu-iodine minerals, Mesozoic marine sedimentary rocks and groundwater are in agreement with previously reported $^{129}I/I$ ratios of marine pore fluids derived from organic material ($200–500 \times 10^{-15}$; Fehn et al., 2007b; Fehn, 2012). Despite the fact that some higher, surface-like values were measured in the nitrates (see previous section and Fig. 5), iodine ratios in nitrate soils from Atacama average $\sim 430 \times 10^{-15}$. Marine sedimentary rocks present a somewhat similar isotopic signature, with shales and calcareous sandstones showing low ratios ($\sim 300–600 \times 10^{-15}$), and one evaporitic rock sample showing a surface-like ratio of 1415×10^{-15}. One groundwater from Antofagasta has an

isotopic ratio of 217×10^{-15} (Fig. 3). Most of these data are significantly lower than surficial values represented by the pre-anthropogenic marine input ratio of 1500×10^{-15}. While the lowest isotopic ratios point toward one or more old and deep organic sources for iodine, the ratios close to 1500×10^{-15} suggest the presence of pre-anthropogenic atmospheric iodine. This large variation observed in the isotopic ratios in Atacama is most likely the result of fluid mixing from different organic and non-organic sources.

Potential sources for organic iodine within an active continental margin include marine sediments (*e.g.*, Snyder and Fehn, 2002) and organic-rich formations in the overlying plate (*e.g.*, Fehn and Snyder, 2003). The Jurassic marine basement, outcropping in the Central Depression and Precordillera of the Atacama region, is formed by a thick, ~1.5 km thick marine sedimentary sequence containing organic rich deposits as shales, richly fossiliferous limestones and calcareous sandstones, and has been proposed as a viable source of organic iodine (Arcuri and Brimhall, 2003; Amilibia et al., 2008; Reich et al., 2013; Pérez-Fodich et al., 2014). On the other hand, sources of pre-anthropogenic atmospheric iodine could correspond to aerosol deposition or meteoric water addition before the onset of the nuclear age (Michalski et al., 2004; Ewing et al., 2006, 2008; Pérez-Fodich et al., 2014).

Fig. 6 shows a mixing diagram where the $^{129}I/I$ ratios in soil and rock samples were plotted *vs.* the reciprocal of iodine concentration. Datapoints in Fig. 6 display an inverse relation between isotopic ratios and iodine concentrations, which provides additional evidence that there is more than one source of iodine in Atacama (Fehn et al., 2007b). Most of the isotopic data range between ~150 and 450×10^{-15}, although a small but significant group with higher ratios is observed. This, together with the wide variation in iodine concentrations suggests that iodine in these reservoirs could have different mixing histories (Lu et al., 2008). In Fig. 6, we identify two different mixing trends and three endmembers (A, B, and C). The "A" endmember corresponds to the point with the lowest isotopic ratio and the highest iodine concentration (nitrate soils and supergene Cu deposits), its isotopic signature is indicative of significant inputs of old organic iodine sources from, for example, the Jurassic marine sequences. The "B" endmember corresponds to the highest isotopic ratio showing the lowest concentration (in this case sample M1A-A; Table 1). Finally, the "C" endmember is characterized by the lowest iodine concentration (sample T4B-A; Table 1). The A–B trend indicates mixing of iodine in nitrate soils/supergene Cu deposits (A) with a largely atmospheric source of $^{129}I/I \sim 1500 \times 10^{-15}$ (B). In contrast, the A–C trend represents interaction between the nitrates/Cu deposits (A) and a possible volcanic source (C) with an isotopic ratio of $\sim 800 \times 10^{-15}$ (Snyder and Fehn, 2002). A large number of datapoints plot in the lower part of the diagram and have isotopic ratios $<450 \times 10^{-15}$, reflecting a stronger influence of the "A" endmember. Although most of the samples do not show any significant preference for a particular trend, five of the six samples from the Tarapacá nitrate soils are in agreement with the A–C trend (Fig. 6).

This analysis suggests that organic-rich (marine sedimentary rocks), volcanic (arc-related) and meteoric (atmospheric) sources are most likely involved in iodine enrichment in Atacama. Of all these sources, the Jurassic marine-sedimentary sequences (*e.g.*, shales, limestones and sandstones) are the most probable source of "old" organic iodine since they have low $^{129}I/I$ ratios (Table 1 and Fig. 2), high organic content, and a widespread regional occurrence upstream in the drainage basin (Mpodozis et al., 2005; Vicente, 2006; Pérez-Fodich et al., 2014). Marine Jurassic rocks in the Precordillera and Central Depression are interpreted as a series of back-arc basins associated with a magmatic arc located westwards along the present-day Coastal Cordillera. In the study area (19°–25°S), the Jurassic geological record to the east is characterized by a thick

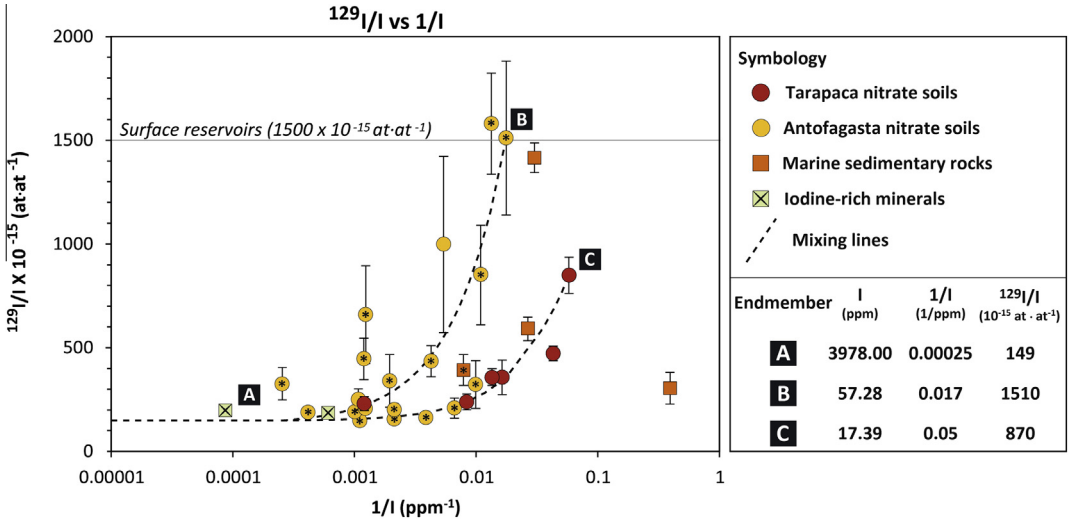

Fig. 6. Iodine mixing diagram. Three endmembers are shown (A, B and C) and two mixing trends (A–B and A–C). See Section 5.2 for detailed discussion. Samples from Chuquicamata were taken from Reich et al. (2013) and selected nitrate soil and marine sedimentary data (*) were taken from Pérez-Fodich et al. (2014).

succession of marine sedimentary deposits composed of fossiliferous limestones, calcareous sandstones and shales, the result of an important marine regression that occurred in the Andean Basin (Marinovic et al., 1995; Vicente, 2006; Oliveros et al., 2012).

5.3. Fluid mixing and timescales of groundwater flow

Despite the fact that large-scale groundwater flow has been recognized to play a fundamental role in leaching halogens from the aforementioned Jurassic marine sequences (*e.g.,* Cameron et al., 2002, 2010; Arcuri and Brimhall, 2003; Reich et al., 2008, 2009b, 2013; Pérez-Fodich et al., 2014), the extent, amount of mixing and timescales of circulation in the Atacama region still remain unconstrained.

In the this section we evaluate the iodine contributions from additional sources such as meteoric water and volcanic fluids, considering also the effects of fissiogenic or "*in situ*" iodine production, which can have a significant impact within the "old" isotopic signal of deep marine fluids hosted by rock formations with significant concentrations of uranium (usually U > 1 ppm, ratios > 1500×10^{-15}, Fabryka-Martin et al., 1989; Snyder et al., 2003). By combining the isotopic data with a geochemical model of fluid mixing, we estimate the timescales of groundwater circulation and mixing trajectories for the sample dataset.

In our conceptual model, iodine formerly resides in the pore waters of the marine sediments in the Jurassic basin. During or after compaction and diagenesis, a fraction of this "old" and organically derived iodine of low $^{129}I/I$ ratio was progressively released from the sediment column and migrated with the fluid. The remaining iodine in the sedimentary rock, measured today in our rock samples from the Jurassic formations was incorporated into the solid fraction, most likely in the carbonate or clay portions. Thus, it is likely that iodine has been subjected to multiple episodes of remobilization from its original sedimentary source by the effect of fluid migration (*e.g.,* deep formation waters), direct leaching, or both.

In order to explore fluid mixing scenarios, we evaluated the evolution of iodine isotopic ratios as a function of time starting with an analog deep pore fluid that represents the "old" iodine source with initial $^{129}I/I = 290 \times 10^{-15}$ and iodine concentration of ~1130 μM (pore fluids hosted in recent marine sediments on the Peru fore-arc, Fehn et al., 2007b). These starting values are used in the absence of $^{129}I/I$ data in marine sediments from the Chilean fore-arc, and are considered representative of marine sediments in a continental margin setting. The black curve in Fig. 7

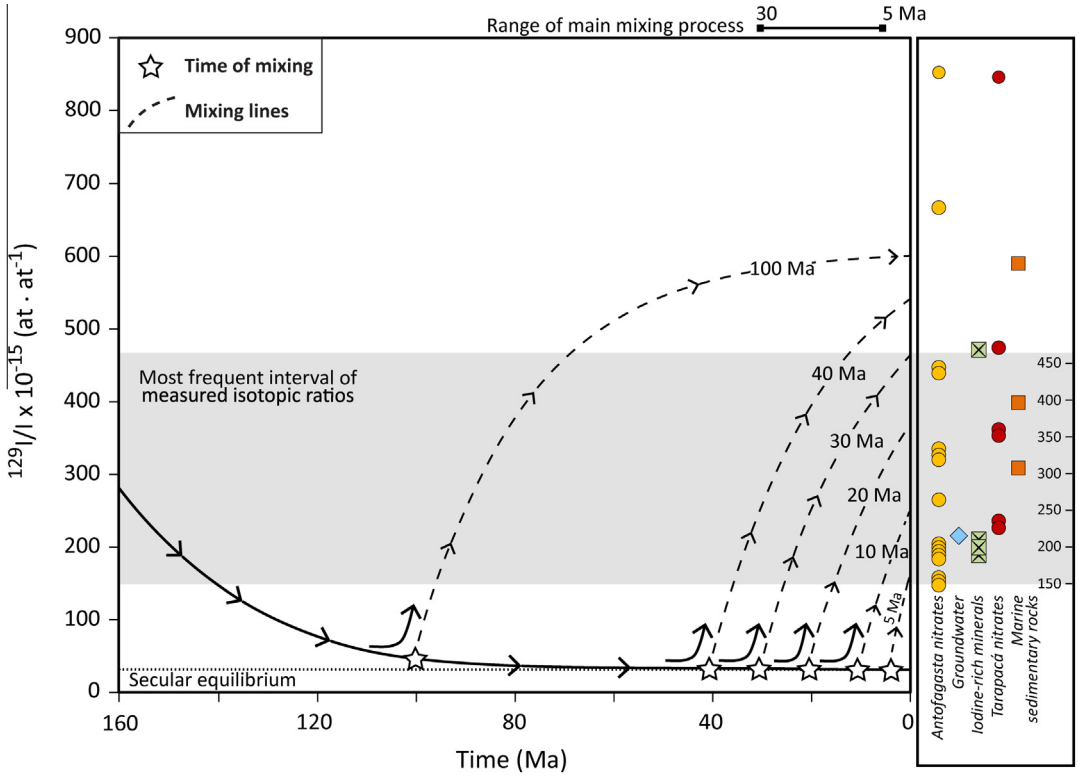

Fig. 7. Geochemical mixing model showing the secular variation of the iodine isotopic ratio of an organically derived deep pore fluid (solid black curve). This source fluid undergoes mixing with volcanic fluids and meteoric water at selected times (stars), and arrows indicate the fluid evolution. Modeled fluid trajectories (dotted curves and arrows) show that fluid mixing episodes (stars) occurring between ~30 and 5 Ma increase the $^{129}I/I$ ratios of the source fluid, explaining the range of present $^{129}I/I$ ratios measured in the Atacama samples (horizontal gray area). Individual samples are shown on the right-hand side. See Sections 5.3 and 5.4 for details. Secular equilibrium is reached at ~80 Ma (dotted horizontal line).

shows the evolution of $^{129}I/I$ ratios in the marine sediment source as a function of time:

$$\frac{^{129}I}{I} = \left(\frac{^{129}I}{I}\right)_i e^{-\lambda_{129}t} + \frac{N_{238}\lambda_{sf}Y_{129}\varepsilon\rho\left\{\frac{(1-\varphi)}{\varphi}\right\}\left\{\frac{\left(1-e^{-\lambda_{129}t}\right)}{\lambda_{129}}\right\}}{N_{127}} \quad (1)$$

The first term on the right-hand side of Eq. (1) corresponds to the cosmogenic decay component, where $(^{129}I/I)_i$ is the initial value (1500×10^{-15}), λ_{129} is the decay constant (4.41×10^{-8} yr^{-1}), and t is the time elapsed since burial of organic matter. The second term corresponds to the fissiogenic or "*in situ*" component, which was included in the model, where $N_{238} = {}^{238}U$ atoms/kg rock, λ_{sf} = spontaneous fission decay constant for ^{238}U (8.5×10^{-17} yr^{-1}; Decarvalho et al., 1982), Y_{129} = spontaneous fission yield of ^{238}U at mass 129 (3×10^{-4}; Hebeda et al., 1987), ε = escape efficiency of ^{129}I from the mineral lattice into the fluid, ρ = rock density, φ = effective porosity, λ_{129} = decay constant for ^{129}I (4.41×10^{-8} yr^{-1}), t = residence time of fluids in contact with the rocks and N_{127} = stable ^{127}I atoms/L fluid. When the term $e^{-\lambda 129}$ goes to zero, secular equilibrium value for ^{129}I is reached. For our model, we considered a shale density of 2.7 g/cm^3 and effective porosity of 0.01 (Young et al., 1991), if $\varphi << 1$, the term $\{(1-\varphi)/\varphi\}$ in Eq. (1) reduces to $(1/\varphi)$. Taken into consideration recent studies in Atacama (Lacassie et al., 2012; Reich et al., 2013), a uranium concentration in the host rocks of 9 ppm was used, and a value for ε of 0.006 was assumed (Fabryka-Martin et al., 1991; Snyder and Fabryka-Martin, 2007).

Considering a minimum age of formation of marine sequences at 160 Ma in the Atacama region (Amilibia et al., 2008; Blanco et al., 2013) and all previous conditions, the secular equilibrium for the iodine isotopic system was reached at ~80 Ma with a ratio of $\sim 35 \times 10^{-15}$ (Fig. 7, dotted horizontal line). Within this scenario, an organically-derived fluid separated from the Jurassic marine basement would have had an $^{129}I/I$ ratio too low (35×10^{-15}) to explain the whole range of $^{129}I/I$ ratios measured in the studied samples (Fig. 7, horizontal gray area and data points for each reservoir), and thus seems unlikely as a sole fluid source for iodine enrichment in Atacama.

The second scenario involved fluid mixing, considering the evidence presented in the Section 5.1 (Fig. 6). Fig. 7 shows segmented lines that represent the evolution of the starting iodine source that, instead of having evolved in a closed system as in the previous scenario, mixed with iodine inputs from additional sources (*i.e.*, meteoric and volcanic sources) at specific times (Fig. 7, white stars). We considered the same deep pore fluid source containing an "old" iodine component ($X_{fw} = 5\%$, $(^{129}I/I)_{fw} = 290 \times 10^{-15}$, $I = 1130$ μM; Fehn et al., 2007b; Reich et al., 2013), that was diluted with a younger fluid (*e.g.*, groundwater) composed of meteoric water ($X_{mw} = 90\%$, $(^{129}I/I)_{mw} = 1500 \times 10^{-15}$, $I = 0.4$ μM; Table 2; Fehn et al., 2007a; Reich et al., 2013) and volcanic fluid ($X_{vw} = 5\%$, $(^{129}I/I)_{vw} = 500 \times 10^{-15}$, $I = 35$ μM; Giggenbach, 1992; Snyder and Fehn, 2002):

$$\left(\frac{^{129}I}{I}\right)_{mix} = \frac{X_{fw}\left(\frac{^{129}I}{I}\right)_{fw}N_{fw}^{127} + X_{mw}\left(\frac{^{129}I}{I}\right)_{mw}N_{mw}^{127} + X_{vw}\left(\frac{^{129}I}{I}\right)_{vw}N_{vw}^{127}}{X_{fw}N_{fw}^{127} + X_{mw}N_{mw}^{127} + X_{vw}N_{vw}^{127}} \quad (2)$$

and

$$N_{127mix} = X_{fw}N_{fw} + X_{vw}N_{vw} + X_{mw}N_{mw} \quad (3)$$

The isotopic evolution of the diluted fluids was modeled using Eq. (1), substituting $(^{129}I/I)_{mix}$ for $(^{129}I/I)_i$ and N_{127mix} for N_{127} (Fig. 7, segmented curves). It is noteworthy to mention that most of the total iodine concentration (~96.8%) is provided by the deep pore fluid source (first term in Eq. (3)), while the volcanic fluid provides about 3% (second term in Eq. (3)), and meteoric water only ~0.2% (third term in Eq. (3)). Therefore, the number of atoms of ^{129}I in the deep pore fluid (~94.7%) is much larger than the number of atoms of ^{129}I in the volcanic fluid (~5%) and meteoric water (~0.3%). Therefore, even though the ratios for meteoric water and volcanic fluids are higher than the ratio for the deep formation waters, the latter will not be seriously affected at the time of mixing.

Thus, the modeled fluid $^{129}I/I$ ratios are in agreement with the measured $^{129}I/I$ ratios in nitrate soils, rock and groundwater samples ($\sim 150–450 \times 10^{-15}$; horizontal gray area in Fig. 7) when mixing or dilution events between the old organic source, and younger groundwater would correspond to a long-term process. Based on the model presented here, we estimate that this process operated between 30 and 5 Ma ago.

5.4. Tectonic, climatic and metallogenic implications

The estimated range of mixing time above (30–5 Ma) is consistent with the climatic, tectonic and hydrologic evolution of the Atacama region during the last 30 million years. Although there is no consensus about the onset of hyperaridity, different authors have reported semiarid climate conditions with rates of precipitation that have decreased progressively from >10 cm/yr (45–15 Ma) to less than 10 mm/yr in the last 10 Ma (Arancibia et al., 2006; Rech et al., 2006; Reich et al., 2009b; Amundson et al., 2012). Regarding tectonic evolution, a relationship between the Andean uplift during the Miocene and the desiccation of the western margin of the Atacama region has been proposed, where tectonic uplift blocked moisture from the South American summer monsoon from entering the Atacama Desert (*e.g.,* Hartley, 2003; Rech et al., 2006). Regardless of the uplift model invoked, there is consensus that progressive deformation events developed since the late Oligocene-early Miocene (~30 Ma, Charrier et al., 2013) would have caused uplift in the central Andes (Hartley, 2003; Garzione et al., 2008; Barnes and Ehlers, 2009). Our estimated mixing times are consistent with a protracted groundwater flow phase between ~30 and 5 Ma, most likely triggered by an increase in the hydraulic potential between the Andes and the Central Depression creating favorable conditions for the development of the groundwater system

(Hoke et al., 2004; Pérez-Fodich et al., 2014). These results are also in agreement with the significant isotopic fractionation of chromium reported by Pérez-Fodich et al. (2014), indicative of intense Cr redox cycling due to groundwater transport from a source in the High Andes to a final sink in the chromium-bearing nitrate soils in the Central Depression. Even though detailed geochemical models are still needed to better constrain the extent of groundwater contribution in terms of dissolved salt species, published data sources (Bale et al., 2002) indicate that reduced species of iodine, chromium, nitrogen and sulfur can be stable in groundwater at near-neutral to slightly alkaline pH conditions that are consistent with those measured in the field (Table 2).

The estimated mixing period reported in this study (30–5 Ma) overlaps with the peak of supergene enrichment of copper in northern Chile, as determined by Ar–Ar dating of supergene minerals giving ages between ~33 and 9 Ma (Alpers and Brimhall, 1988; Sillitoe and McKee, 1996). However, our data suggest the involvement of groundwater flow until ~5 Ma, in agreement with more recent studies that constrain the age span of supergene enrichment in Atacama. Radiometric data compiled by Hartley and Rice (2005) show an increase in the frequency of supergene ages until ~6 Ma, while Arancibia et al. (2006) proposed that supergene oxidation of copper deposits ceased ca. 5 Ma as result of climate desiccation in the southern Atacama Desert. Along the same line, Reich et al. (2009b) suggest that the "meteoric" supergene enrichment of copper, driven by downward penetration of surficial waters, waned after 9 Ma and ceased at ~5 Ma. As a result of desiccation, the meteoric supergene stage was followed by an atacamite-forming supergene stage, driven by the interaction of old and saline brines with copper minerals under conditions of increasing aridity (Reich et al., 2008). Therefore, during this interval (30–5 Ma), large-scale circulation of groundwater and deep fluids existed in the Atacama region, which would have allowed continuous mixing for at least 25 Ma (Fig. 7).

The analysis presented here focuses mostly in samples showing low iodine isotopic ratios (from ~150 to 450×10^{-15}), which are in fact the most abundant. However, the presence of a few datapoints with higher isotopic ratios ($>1000 \times 10^{-15}$; Fig. 3) cannot be explained exclusively by an "old" meteoric water influence, because this would imply mixing episodes before the deposition of the Jurassic organic source (>160 Ma) to achieve such high ratios. Therefore, "young" meteoric inputs seem more likely to explain the higher, near-surface isotopic ratios. Such ratios are indicative of recent fluid mixing events between an organic source (*e.g.*, marine sedimentary rocks) and meteoric water younger than 5 Ma, probably in a lesser extent than other components previously described. This interpretation is in agreement with studies proposing that modern hyperarid conditions would have settled since late Pliocene to early Pleistocene (*e.g.,* Hartley and Chong, 2002; Ewing et al., 2006). Pedological evidence of salt distribution in Pliocene soils near Aguas Blancas suggests large and infrequent storms that infiltrated gentle alluvial fans (Ewing et al., 2006; Amundson et al., 2012). The most recent Atacama landform ages of ~2 Ma, determined using cosmogenic and Ar–Ar dating, point toward a cessation of fluvial features that are related to an arid-hyperarid rainfall transition (Ewing et al., 2006; Amundson et al., 2012). Even though surface run-off in the last ~2 Ma was infrequent, and most likely related to flooding events associated with increased precipitation in the High Andes, there is geological evidence of subsequent groundwater recharge episodes in the Atacama Desert (*e.g.*, >15.4–9 ka, Rech et al., 2002; ~16–13 ka, Nester et al., 2007; ~16–10, Quade et al., 2008). The presence of recent groundwater flow is also supported by chlorine-36 data in atacamite ($Cu_2Cl(OH)_3$) from copper deposits in the region. Atacamite samples from supergene assemblages in Cu deposits from the Precordillera to the Coastal Range show very low ^{36}Cl-to-Cl ratios (11×10^{-15} to 28×10^{-15} at·at^{-1}), comparable to previously reported ^{36}Cl-to-Cl ratios of deep formation waters and old groundwaters (Reich et al., 2008). Chlorine-36 data in atacamite indicate that the chlorine in saline waters related to atacamite formation is old (>1.5 Ma) but that atacamite formation occurred more recently (<1.5 Ma). This strongly suggests that significant groundwater mixing and circulation events have occurred intermittently since the onset of hyperaridity (Nester et al., 2007; Reich et al. (2009a,b); Saez et al., 2012).

Results from this study show that the anomalous iodine enrichment in Atacama is evidence of extensive and protracted fluid flow within an active continental margin. The extent of fluid circulation is reflected by the remobilization of iodine from volcanic fluids and marine sedimentary rocks in the Precordillera and volcanic arc. This groundwater, originally composed of low salinity regional fluids of meteoric origin and fluids of volcanic origin, diluted the "old" organic iodine in marine sequences along its flow path and increased the ^{129}I/I ratios during a significant period of time (between ~30 and 5 Ma). Iodine fixation in soils/sediments and precipitation of supergene Cu minerals was possible due to the interaction between these mixed fluids and preexisting deposits under increasing tectonic uplift and desiccation conditions, with significant (and highly variable) inputs of atmospheric, eolian and sea spray contributions (Hoke et al., 2004; Pérez-Fodich et al., 2014). Even though increased aridity resulted in the preservation of iodine and other soluble components, detailed analyses of soil profiles suggest subsequent *in situ* mixing processes with pre-anthropogenic meteoric water, which have increased the isotopic ratios to values around 1500×10^{-15} after 5 Ma.

It is noteworthy that old and deep groundwater has played an essential role not only in the continental cycle of iodine in Atacama, but also has had an impact on metal speciation, transport and mineral precipitation in supergene zones, and on the development of geochemical soil anomalies above copper deposits. This has been documented by several authors, including Cameron et al. (2002, 2004, 2007, 2008, 2010), Cameron and Leybourne (2005), Palacios et al. (2005), Leybourne and Cameron (2008), and Reich et al. (2008, 2009b, 2013). The involvement of a persistent regional groundwater flow in Atacama, supported by stable isotope studies (*e.g.*, δ^{37}Cl in atacamite

at Radomiro Tomic, Arcuri and Brimhall, 2003; δD and $\delta^{18}O$ in groundwaters at Spence, Leybourne and Cameron, 2006b; Pérez-Fodich et al., 2014), strongly suggests that the regional-scale iodine (and supergene copper) enrichment in Atacama is tied to large-scale groundwater circulation over a scale of millions-of-years.

6. CONCLUSIONS

The results reported in this study show that iodine enrichment in the Atacama Desert of northern Chile is widespread and varies significantly between reservoirs. Most iodine isotopic ratios of soils, rocks and waters reported in this study ($\sim$150–1580 $\times$ 10^{-15}) are lower than the pre-anthropogenic surface ratio of 1500×10^{-15}, strongly suggesting that iodine in the studied reservoirs is derived from different sources undergoing different mixing histories. Our geochemical mixing models confirm that the most significant rich-organic source for the widespread iodine enrichment in the Atacama region is the Jurassic marine basement, with variable degrees of meteoric water and volcanic fluid inputs that have occurred extensively over a protracted period ($\sim$30–5 Ma).

Our data show that the iodine isotopic system ($^{129}I/I$) can be successfully used in continental settings as a paleotracer of water circulation over tens-of-million year timescales. Since large-scale fluid migration is now recognized as playing a major role in virtually all geologic processes (Garven et al., 2010) including metal transport and deposition (*e.g.*, Leybourne and Cameron, 2006b, 2008), landscape evolution (*e.g.*, Hoke et al., 2004), geothermal and hydrothermal recharge (*e.g.*, Giggenbach, 1978; Snyder et al., 2002) and halogen recycling through subduction zones (*e.g.*, Kendrick et al., 2011, 2012), the results presented in this study shed new lights on timescales of fluid flow and its relations with the climatic, hydrologic and geodynamic history of active continental margins.

ACKNOWLEDGMENTS

Financial support for this study was provided by FONDECYT grant 1100014 to Martin Reich. Additional support by FONDAP project 15090013 "Centro de Excelencia en Geotermia de los Andes, CEGA" and MSI grant "Millennium Nucleus for Metal Tracing Along Subduction", NC130065 is acknowledged. Fernanda Álvarez thanks CONICYT for providing support through a Ph.D. scholarship ("Programa de Becas de Doctorado"). We thank the AMS group at PrimeLab, Purdue University for carrying out the ^{129}I measurements. Finally, we acknowledge Constanza Nicolau for her help with fieldwork logistics. We also acknowledge Associate Editor Brian Stewart, and thoughtful and constructive comments by three anonymous reviewers.

REFERENCES

Alpers C. N. and Brimhall G. H. (1988) Middle Miocene climatic change in the Atacama Desert, northern Chile: evidence from supergene mineralization at La Escondida. *Geol. Soc. Am. Bull.* **100**, 1640–1656.

Amilibia A., Sàbat F., McClay K. R., Muñoz J. A., Roca E. and Chong G. (2008) The role of inherited tectono-sedimentary architecture in the development of the central Andean mountain belt: insights from the Cordillera de Domeyko. *J. Struct. Geol.* **30**(12), 1520–1539.

Amundson R., Dietrich W., Bellugi D., Ewing S., Nishiizumi K., Chong G., Owen J., Finkel R., Heimsath A. and Stewart B. (2012) Geomorphologic evidence for the late Pliocene onset of hyperaridity in the Atacama Desert. *Geol. Soc. Am. Bull.* **124**, 1048–1070.

Andrews J. N., Davis S. N., Fabryka-Martin J., Fontes J. C., Lehmann B. E., Loosli H. H., Michelot J.-L., Moser H., Smith B. and Wolf M. (1989) The in situ production of radioisotopes in rock matrices with particular reference to the Stripa granite. *Geochim. Cosmochim. Acta* **53**, 1803–1815.

Angermann D., Klotz J. and Reigber C. (1999) Space-geodetic estimation of the Nazca-South America Euler vector. *Earth Planet. Sci. Lett.* **171**, 329–334.

Arancibia G., Matthews S. J. and De Arce C. P. (2006) K-Ar and Ar-40/Ar-39 geochronology of supergene processes in the Atacama Desert, northern Chile: tectonic and climatic relations. *J. Geol. Soc. London* **163**, 107–118.

Aravena R. (1995) Isotope hydrology and geochemistry of northern Chile groundwaters. *Bull. Inst. Fr. Etudes Andin.* **24**, 495–503.

Aravena R., Suzuki O., Peña H., Pollastri A., Fuenzalida H. and Grilli A. (1999) Isotopic composition and origin of the precipitation in northern Chile. *Appl. Geochem.* **14**, 411–422.

Arcuri T. and Brimhall G. (2003) The chloride source for atacamite mineralization at the Radomiro Tomic porphyry copper deposit, northern Chile. *Econ. Geol.* **98**, 1667–1681.

Bale C. W., Chartrand P., Degtrev S. A., Eriksson G., Hack K., Ben Mahfoud R., Melancon J., Pelton A. D. and Petersen S. (2002) FactSage thermochemical software and databases. *Calphad* **26**, 189–228.

Bao H. M. and Gu B. (2004) Natural perchlorate has a unique oxygen isotope signature. *Environ. Sci. Technol.* **38**, 5073–5077.

Barnes J. B. and Ehlers T. A. (2009) End member models for Andean Plateau uplift. *Earth Sci. Rev.* **97**, 105–132.

Betancourt J. L., Latorre C., Rech J. A., Rylander K. A. and Quade J. (2000) A 22,000-year record of monsoonal precipitation from northern Chile's Atacama Desert. *Science* **289**, 1542–1546.

Blanco N., Vásquez P., Sepúlveda F., Tomlinson A., Quezada A. and Ladino M. (2013) Levantamiento geológico para el fomento de la exploración de recursos minerales e hídricos de la Cordillera de la Costa, Depresión Central y Precordillera de la región de Tarapacá (20°–21°S). Servicio Nacional de Geología y Minería, Santiago.

Böhlke J. K., Ericksen G. E. and Revesz K. (1997) Stable isotope evidence for an atmospheric origin of desert nitrate deposits in northern Chile and southern California, USA. *Chem. Geol.* **136**, 135–152.

Bottomley D. J., Renaud R., Kotzer T. and Clark I. D. (2002) Iodine-129 constraints on residence times of deep marine brines in the Canadian Shield. *Geology* **30**, 587–590.

Broecker W. S. and Peng T. H. (1982) *Tracers in the Sea*. Eldigio, Palisades, NY, pp. 690.

Brüggen J. (1938) El salitre. *Sociedad Nacional de Minería, Boletín Minero* **50**, 737–754.

Cameron E. M. and Leybourne M. I. (2005) Relationship between groundwater chemistry and soil geochemical anomalies at the Spence copper porphyry deposit, Chile. *Geochem-Explor. Env.* **5**, 135–145.

Cameron E. M., Leybourne M. I. and Kelley D. L. (2002) Exploring for deeply covered mineral deposits: formation of

geochemical anomalies in northern Chile by earthquake-induced surface flooding of mineralized groundwaters. *Geology* **30**, 1007–1010.

Cameron E. M., Hamilton S. M., Leybourne M. I., Hall G. E. M. and McClenaghan M. B. (2004) Finding deeply buried deposits using geochemistry. *Geochem-Explor. Env. A.* **4**, 7–32.

Cameron E. M., Leybourne M. I. and Palacios C. (2007) Atacamite in the oxide zone of copper deposits in northern Chile: involvement of deep formation waters? *Miner. Deposita* **42**, 205–218.

Cameron E. M., Leybourne M. I., Palacios C. and Reich M. (2008) Geochemical exploration and metallogenic studies, northern Chile. *Geosci. Can.* **35**, 97–107.

Cameron E. M., Leybourne M. I., Reich M. and Palacios C. (2010) Geochemical anomalies in northern Chile as a surface expression of the extended supergene metallogenesis of buried copper deposits. *Geochem-Explor. Env.* **10**, 1–14.

Charrier R., Hérail G., Pinto L., García M., Riquelme R., Farías M. and Muñoz N. (2013) Cenozoic tectonic evolution in the Central Andes in northern Chile and west central Bolivia: implications for paleogeographic, magmatic and mountain building evolution. *Int. J. Earth. Sci.* **102**, 235–264.

Chong G. (1994) The nitrate deposits of Chile. In *Tectonics of the Southern Central Andes: Structure and Evolution of an Active Continental Margin* (eds. E. Scheuber, K. J. Reutter and P. J. Wigger). Springer, pp. 303–316.

Coira B., Davidson J., Mpodozis C. and Ramos V. A. (1982) Tectonic and magmatic evolution of the Andes of northern Argentina and Chile. In *Magmatic Evolution of the Andes* (ed. E. Linares). Earth-Sci. Rev., Special Issue 18, 303–332.

Cortés J. (2000) Hoja Palestina, Región de Antofagasta. Servicio Nacional de Geología y Minería, Mapas Geológicos 19, 1 mapa escala 1:100.000. Santiago.

Decarvalho H. G., Martins J. B., Medeiros E. L. and Tavares O. A. P. (1982) Decay constant for the spontaneous-fission process in ^{238}U. *Nucl. Instrum. Methods* **197**, 417–426.

DeMets C., Gordon R. G., Argus D. F. and Stein S. (1994) Effect of recent revisions to the geomagnetic reversal timescale. *Geophys. Res. Lett.* **21**, 2191–2194.

Dorsaz J., Gironás J., Escauriaza C. and Rinaldo A. (2013) The geomorphometry of endorheic drainage basins: implications for interpreting and modelling their evolution. *Earth Surf. Proc. Land.* **38**, 1881–1896.

Elderfield H. and Truesdale V. W. (1980) On the biophilic nature of iodine in seawater. *Earth Planet. Sci. Lett.* **50**, 105–114.

Ericksen G. E. (1961) Rhyolite tu, a source of the salts of northern Chile. U.S. Geol. Surv. Prof. Paper 424-C.

Ericksen G. E. (1981) Geology and origin of the Chilean nitrate deposits. U.S. Geol. Surv. Prof. Paper 1188-B. Unites States Government Printing Office, Washington.

Ericksen G. E. (1983) The Chilean nitrate deposits. *Am. Sci.* **71**, 366–374.

Ewing S. A., Sutter B., Amundson R., Owen J., Nishiizumi K., Sharp W., Cliff S. S., Perry K., Dietrich W. E. and McKay C. P. (2006) A threshold in soil formation at earth's arid-hyperarid transition. *Geochim. Cosmochim. Acta* **70**, 5293–5322.

Ewing S. A., Michalski G., Thiemens M., Quinn R. C., Macalady J. L., Kohl S., Wankel S. D., Kendall C., MacKay C. P. and Amundson R. (2007) Rainfall limit of the N cycle on earth. *Global Biogeoche. Cy.* **21**, GB3009.

Ewing S. A., Yang W., DePaolo D. J., Michalski G., Kendall C., Stewart B., Thiemans M. and Amundson R. (2008) Non-biological fractionation of Ca isotopes in soils of the Atacama Desert, Chile. *Geochim. Cosmochim. Acta* **72**, 1096–1110.

Fabryka-Martin J., Bentley H., Elmore D. and Airey P. L. (1985) Natural I-129 as an environmental tracer. *Geochim. Cosmochim. Acta* **49**, 337–347.

Fabryka-Martin J. T., Davis S. N., Elmore D. and Kubik P. W. (1989) In situ production and migration of ^{129}I in the Stripa granite, Sweden. *Geochim. Cosmochim. Acta* **53**, 1817–1823.

Fabryka-Martin J., Whittemore D. O., Davis S. N., Kubik P. W. and Sharma P. (1991) Geochemistry of halogens in the Milk River aquifer, Alberta, Canada. *Appl. Geochem.* **6**, 447–464.

Fehn U. (2012) Tracing Crustal Fluids: Applications of Natural ^{129}I and ^{36}Cl. *Annu. Rev. Earth Pl. Sc.* **40**, 45–67.

Fehn U. and Snyder G. T. (2005) Residence times and source ages of deep crustal fluids: interpretation of ^{129}I and ^{36}Cl results from the KTB-VB drill site. *Germany. Geofl.* **5**, 42–51.

Fehn U., Holdren G. R., Elmore D., Brunelle T., Teng R. and Kubik P. W. (1986) Determination of natural and anthropogenic I-129 in marine sediments. *Geophys. Res. Lett.* **13**, 137–139.

Fehn U., Tullai-Fitzpatrick S., Teng R. T. D., Gove H. E., Kubik P. W., Sharma P. and Elmore D. (1990) Dating of oil field brines using ^{129}I. *Nucl. Instrum. Methods Phys. Res.* **52**, 446–450.

Fehn U., Peters E. K., Tullai-Fitzpatrick S., Kubik P. W., Sharma P., Teng R. T. D., Gove H. E. and Elmore D. (1992) ^{129}I and ^{36}Cl concentrations in waters of the eastern Clear Lake area, California: residence times and source ages of hydrothermal fluids. *Geochim. Cosmochim. Acta* **56**, 2069–2079.

Fehn U., Snyder G. T. and Egeberg P. K. (2000) Dating of pore waters with ^{129}I. Relevance for the origin of marine gas hydrates. *Science* **289**, 2332–2335.

Fehn U. and Snyder G. T. (2003) Origin of iodine and ^{129}I in volcanic and geothermal fluids from the North Island of New Zealand: implications for subduction zone processes. *Soc. Econ. Geol. Spec. Publ.* **10**, 159–170.

Fehn U., Snyder G. T., Wallmann K., Hensen C. and Lu Z. (2004) Fluid flow in the main and fore arc of Central America: ^{129}I as tracer of subduccion processes. AGU Fall Meeting, San Francisco, December 2004. EOS Trans. AGU, 85 (47) F1851.

Fehn U., Moran J. E., Snyder G. T. and Muramatsu Y. (2007a) The initial ^{129}I/I ratio and the presence of "old" iodine in continental margins. *Nucl. Instrum. Meth. B.* **259**, 496–502.

Fehn U., Snyder G. T. and Muramatsu Y. (2007b) Iodine as a tracer of organic material: ^{129}I results from gas hydrate systems and fore arc fluids. *J. Geochem. Explor.* **95**, 66–80.

Fiesta B. (1966) El origen del salitre de Chile. *Bol. Soc. Esp. Hist. Nat. Geol.* **64**, 47–56.

Forbes D. (1861) On the geology of Bolivia and southern Perú. *Q. J. Geol. Soc. London* **17**, 7–62.

Frohlich K., Ivanovich M., Hendry M. J., Andrews J. N., Davis S. N., Drimmie R. J., Fabryka-Martin J., Florkowski T., Fritz P., Lehmann B., Loosli H. H. and Nolte E. (1991) Application of isotopic methods to dating of very old groundwaters: Milk River aquifer, Alberta. *Canada. Appl. Geochem.* **6**, 465–472.

Gale H. S. (1912) Nitrate deposits. *U.S. Geological Survey Bull.* **523**, 19–23.

Garzione C. N., Hoke G. D., Libarkin J. C., Whiters S., MacFadden B., Eiler J., Ghosh P. and Mulch A. (2008) Rise of the Andes. *Science* **320**, 1304–1307.

Garreaud R. and Aceituno P. (2001) Interannual rainfall variability over the South American Altiplano. *J. Climate* **14**, 2779–2789.

Garreaud R., Molina A. and Farias M. (2010) Andean uplift and Atacama hyperaridity: a climate modeling perspective. *Earth Planet. Sci. Lett.* **292**, 39–50.

Garven G., Manning C. E. and Yardley B. W. D. (2010) Frontiers in geofluids: editorial. *Geofluids* **10**, 1–2.

Gayó E. M., Latorre C., Jordan T. E., Nester P. L., Estay S. A., Ojeda K. F. and Santoro C. M. (2012) Late quaternary hydrological and ecological change in the hyperarid core of the Northern Atacama Desert (~21°S). *Earth Sci. Rev.* **113**, 120–140.

Giggenbach W. (1978) The isotope composition of waters from the El Tatio geothermal field, northern Chile. *Geochim. Cosmochim. Acta* **42**, 979–988.

Giggenbach W. F. (1992) Isotopic shifts in waters from geothermal and volcanic systems along convergent plate boundaries and their origin. *Earth Planet. Sci. Lett.* **113**, 495–510.

Gilfedder B. S., Lai S. C., Petri M., Biester H. and Hoffmann T. (2008) Iodine speciation in rain, snow and aerosols. *Atmos. Chem. Phys.* **8**, 6069–6084.

Grossling B. F. and Ericksen G. E. (1971) Computer studies of the composition of Chilean nitrate ores: data reduction, basic statistics, and correlation analysis. *U.S. Geol. Surv. Open File Rep.*, 1519.

Hartley A. J. (2003) Andean uplift and climate change. *J. Geol. Soc. Lond.* **160**, 7–10.

Hartley A. J. and Chong G. (2002) Late Pliocene age for the Atacama Desert: implications for the desertification of western South America. *Geology* **30**, 43–46.

Hartley A. J. and Rice C. M. (2005) Controls on supergene enrichment of porphyry copper deposits in the Central Andes: a review and discussion. *Miner. Deposita* **40**, 515–525.

Hebeda E. H., Schulz L. and Freundel M. (1987) Radiogenic, fissiogenic, and nucleogenic noble-gases in zircons. *Earth Planet. Sci. Lett.* **85**, 79–90.

Hervé M., Marinovic N., Mpodozis C. and Smoje I. (1991) Mapa Geológico de la Hoja Sierra de Varas (1:100.000), Región de Antofagasta. Servicio Nacional de Geología y Minería, Documento de Trabajo 2.

Hoke G. D., Isacks B. L., Jordan T. E. and Yu J. S. (2004) Groundwater-sapping origin for the giant quebradas of northern Chile. *Geology* **32**, 605–608.

Houston J. (2002) Groundwater recharge through an alluvial fan in the Atacama Desert, northern Chile: mechanisms, magnitudes and causes. *Hydrol. Proc.* **16**, 3019–3035.

Houston J. (2006) The great Atacama flood of 2001 and implications for Andean hydrology. *Hydrol. Proc.* **20**, 591–610.

Houston J. and Hartley A. J. (2003) The Central Andean west-slope rainshadow and its potential contribution to the origin of hyper-aridity in the Atacama Desert. *Int. J. Climatol.* **23**, 1453–1464.

Jarrell O. (1939) Marshite and other minerals from Chuquicamata, Chile. *Am. Miner.* **24**, 629–635.

Jarrell O. (1944) Oxidation at Chuquicamata, Chile. *Econ. Geol.* **39**, 251–286.

Kelley D. L., Hall G. E., Closs G., Hamilton I. C. and McEwen R. M. (2003) The use of partial extraction geochemistry for copper exploration in northern Chile. *Geochem. Explor. Environ. Analysis* **3**, 85–104.

Kendrick M. A., Scambelluri M., Honda M. and Phillips D. (2011) High abundances of noble gas and chlorine delivered to the mantle by serpentinite subduction. *Nat. Geosci.* **4**, 807–812.

Kendrick M. A., Woodhead J. D. and Kamenetsky V. S. (2012) Tracking halogens through the subduction cycle. *Geology* **40**, 1075–1078.

Küpper F. C., Carpenter L. J., McFiggans G. B., Palmer C. J., Waite T. J., Boneberg E. M., Woitsch S., Weiller M., Abela R., Grolimundi D., Potin P., Butler A., Luther, III, G. W., Kroneck P. M. H., Meyer-Klaucke W. and Feiters M. C. (2008) Iodide accumulation provides kelp with an inorganic antioxidant impacting atmospheric chemistry. *P. Natl. Acad. Sci. U.S.A.* **105**(19), 6954–6958.

Lacassie J. P., Astudillo F., Baeza L., Castillo P., Figueroa M., Muñoz N. and Ramírez C. (2012) Geoquímica de sedimentos de la Hoja Iquique, Región de Tarapacá. Servicio Nacional de Geología y Minería, Carta Geológica de Chile, Serie Geoquímica 1, 1 DVD versión 1.0, que contiene 1 mapa interactivo para 59 elementos químicos escala 1:250.000, 1 texto (41p.) y 2 anexos. Santiago.

Latorre C., Santoro C., Ugalde P., Gayo E., Osorio D., Salas-Egaña C., De Pol-Holz R., Joly D. and Rech J. (2013) Late Pleistocene human occupation of the hyperarid core in the Atacama Desert, northern Chile. *Quat. Sci. Rev.* **77**, 19–30.

Leybourne M. I. and Cameron E. M. (2006a) Composition of soils and ground waters at the Pampa del Tamarugal, Chile: anatomy of a fossil geochemical anomaly derived from a distant porphyry copper deposit. *Econ. Geol.* **101**, 1569–1581.

Leybourne M. I. and Cameron E. M. (2006b) Composition of groundwaters associated with porphyry-Cu deposits, Atacama Desert, Chile: elemental and isotopic constraints on water sources and water-rock reactions. *Geochim. Cosmochim. Acta* **70**, 1616–1635.

Leybourne M. I. and Cameron E. M. (2008) Source, transport, and fate of rhenium, selenium, molybdenum, arsenic, and copper in groundwater associated with porphyry-Cu deposits, Atacama Desert, Chile. *Chem. Geol.* **247**, 208–228.

Leybourne M. I., Cameron E. M., Reich M., Palacios C., Faure K. and Johannesson K. H. (2013) Stable isotopic composition of soil calcite (O, C) and gypsum (S) overlying Cu deposits in the Atacama Desert, Chile: implications for mineral exploration, salt sources, and paleoenvironmental reconstruction. *Appl. Geochem.* **29**, 55–72.

Lu Z., Hensen C., Fehn U. and Wallmann K. (2008) Halogen and ^{129}I systematics in gas hydrate fields at the northern Cascadia margin (IODP Expedition 311): insights from numerical modeling. *Geochem. Geophys. Geosyst.* **9**, Q10006.

Lu Z., Tomaru H. and Fehn U. (2011) Comparison of iodine dates from mud volcanoes and gas hydrate occurrences: relevance for the movement of fluids and methane in active margins. *Am. J. Sci.* **311**, 632–650.

Magaritz M., Aravena R., Peña H., Suzuki O. and Grilli A. (1990) Source of Ground Water in the Deserts of northern Chile: Evidence of Deep Circulation of Ground Water from the Andes. *Ground Water* **28**, 513–517.

Marinovic N. and García M. (1999) Hoja Pampa Unión, Región de Antofagasta. Servicio Nacional de Geología y Minería, Mapas Geológicos 9 (escala1:100.000), Santiago.

Marinovic N., Smoje L., Maksaev V., Hervé M. and Mpodozis C. (1995) Hoja Aguas Blancas, Región de Antofagasta. *Servicio Nacional de Geología y Minería, Carta Geológica de Chile*(70), 150.

Martin J. B., Gieskes J. M., Torres M. and Kastner M. (1993) Bromine and iodine in Peru margin sediments and pore fluids: implications for fluid origins. *Geochim. Cosmochim. Acta* **57**, 4377–4389.

McKay C. P., Friedmann E. I., Gomez-Silva B., Caceres-Villanueva L., Andersen D. T. and Landheim R. (2003) Temperature and moisture conditions for life in the extreme arid region of the Atacama Desert: four years of observations including the El Niño of 1997–1998. *Astrobiology* **3**, 393–406.

Michalski G., Bohlke J. K. and Thiemens M. (2004) Long term atmospheric deposition as the source of nitrate and other salts in the Atacama Desert, Chile: New evidence from massindependent oxygen isotopic compositions. *Geochim. Cosmochim. Acta* **68**, 4023–4038.

Moran J. E., Fehn U. and Hanor J. S. (1995) Determination of source ages and migration patterns of brines from the U.S. Gulf Coast basin using ^{129}I. *Geochim. Cosmochim. Acta* **59**, 5055–5069.

Moran J. E., Fehn U. and Teng R. T. D. (1998) Variations in $^{129}I/^{127}I$ ratios in recent marine sediments: Evidence for a fossil organic component. *Chem. Geol.* **152**, 193–203.

Mpodozis C., Arriagada C., Basso M., Roperch P., Cobbold P. and Reich M. (2005) Late Mesozoic to Paleogene stratigraphy of the Salar de Atacama Basin, Antofagasta, Northern Chile: Implications for the tectonic evolution of the Central Andes. *Tectonophysics* **399**, 125–154.

Mueller G. (1960) The theory of formation of north Chilean nitrate deposits through (capillary concentration). International Geological Congress, 21st, Copenhagen 1960. *Reposrt* **1**, 76–86.

Muramatsu Y. and Wedepohl K. H. (1998) The distribution of iodine in the earth's crust. *Chem. Geol.* **147**, 201–216.

Nester P. L., Gayo E., Latorre C., Jordan T. E. and Blanco N. (2007) Perennial stream discharge in the hyperarid Atacama Desert of northern Chile during the latest Pleistocene. *P. Natl. Acad. Sci. USA* **104**, 19724–19729.

Noellner C. N. (1867) Über die Entstehung der Salpeter-und Boraxlager in Peru. *J. Prakt. Chem.* **102**, 459–464.

Oliveros V., Labbé M., Rossel P., Charrier R. and Encinas A. (2012) Late Jurassic paleogeograhic evolution of the Andean back-arc basin: New constrains from the Lagunillas Formation, northern Chile (27°30'-28°30'S). *J. S. Am. Earth Sci.* **37**, 25–40.

Oyarzún J. and Oyarzún R. (2007) Massive volcanism in the Altiplano-Puna Volcanic Plateau and formation of the huge Atacama Desert Nitrate Deposits: A case for thermal and electric xation of atmospheric nitrogen. *Int. Geol. Rev.* **49**, 962–968.

Palacios C., Guerra N., Townley B., Lahsen A. and Parada M. (2005) Copper geochemistry in salt from evaporite soils, coastal range of the Atacama Desert, northern Chile: an exploration tool for blind Cu deposits. *Geochem. Explor. Environ. Analysis A* **5**, 371–378.

Pardo-Casas F. and Molnar P. (1987) Relative motion of the Nazca (Farallon) and South American Plate since Late Cretaceous time. *Tectonics* **6**, 233–248.

Penrose, Jr, R. A. F. (1910) The nitrate deposits of Chile. *J. Geol.* **18**, 1–32.

Pérez-Fodich A., Reich M., Álvarez F., Snyder G. T., Schoenberg R., Vargas G., Muramatsu Y. and Fehn U. (2014) Climate change and tectonic uplift triggered the formation of the Atacama Desert's giant nitrate deposits. *Geology* **42**, 251–254.

Pissis A. (1878) Report upon the Desert of Atacama, its geology and mineral products. In London, Taylor and Francis (eds.) Nitrate and guano deposits in the Desert of Atacama, 1–30.

Pueyo J. C., Chong G. and Vega M. (1998) Mineralogy and parental brine evolution in the Pedro de Valdivia nitrate deposit, Antofagasta. *Chile. Rev. Geol. Chile* **25**, 3–15.

Quade J., Rech J. A., Betancourt J. L., Latorre C., Quade B., Rylander K. A. and Fisher T. (2008) Paleowetlands and regional climate change in the central Atacama Desert, northern Chile. *Quat. Res.* **69**, 343–360.

Rao U. and Fehn U. (1999) Sources and reservoirs of anthropogenic iodine-129 in western New York. *Geochim. Cosmochim. Acta* **63**, 1927–1938.

Rech J. A., Quade J. and Betancourt J. L. (2002) Late Quaternary paleohydrology of the central Atacama Desert (lat 22 degrees-24 degrees S). *Chile. Geol. Soc. Am. Bull.* **114**, 334–348.

Rech J. A., Quade J. and Hart W. S. (2003) Isotopic evidence for the source of Ca and S in soul gypsum, anhydrite and calcite in the Atacama Desert. *Chile. Geochim. Cosmochim. Acta* **67**, 575–586.

Rech J. A., Currie B. S., Michalski G. and Cowan A. M. (2006) Neogene climate change and uplift in the Atacama Desert, Chile. *Geology* **34**, 761–764.

Reich M., Palacios C., Parada M. A., Fehn U., Cameron E. M., Leybourne M. I. and Zúñiga A. (2008) Atacamite formation by deep saline waters in copper deposits from the Atacama Desert, Chile: Evidence from fluid inclusions, groundwater geochemistry, TEM, and ^{36}Cl data. *Miner. Deposita* **43**, 663–675.

Reich M., Palacios C., Alvear M., Cameron E. M., Leybourne M. I. and Deditius A. (2009a) Iodine-rich waters involved in supergene enrichment of the Mantos de la Luna argentiferous copper deposit, Atacama Desert. *Chile. Miner. Deposita* **44**, 719–722.

Reich M., Palacios C., Vargas G., Luo S., Cameron E. M., Leybourne M. I., Parada M. A., Zúñiga A. and You C. F. (2009b) Supergene enrichment of copper deposits since the onset of modern hyperaridity in the Atacama Desert. *Chile. Miner. Deposita* **44**, 497–504.

Reich M., Snyder G. T., Álvarez F., Pérez A., Palacios C., Vargas G., Cameron E. M., Muramatsu Y. and Fehn U. (2013) Using iodine isotopes to constrain supergene fluid sources in arid regions: insights from the Chuquicamata oxide blanket. *Econ. Geol.* **108**, 163–171.

Rundel P. W., Dillon M. O., Palma B., Mooney H. A., Gulmon S. L. and Ehleringer J. R. (1991) The phytogeography and ecology of the coastal Atacama and Peruvian deserts. *ALISO* **13**, 1–49.

SERNAGEOMIN (2003) Geologic map of Chile, digital version, scale 1:1000000.

Sharma P., Bourgeois M., Elmore D., Granger D., Lipschutz M. E., Ma X., Miller T., Mueller K., Rickey F., Simms P. and Vogt S. (2000) PRIME lab AMS performance, upgrades and research applications. *Nucl. Instr. Meth. B.* **172**, 112–123.

Saez A., Cabrera L. l., Garcés M., Bogaard P., Jensen A. and Gimeno G. (2012) The stratigraphic record of changing hyperaridity in the Atacama desert over the last 10 Ma. *Earth Planet. Sci. Lett.* **355**, 32–38.

Schink D. R., Santschi P. H., Corapcioglu P., Sharma P. and Fehn U. (1995) ^{129}I in Gulf of Mexico waters. *Earth Planet. Sci. Lett.* **135**, 131–138.

Snyder G. T. and Fehn U. (2002) Origin of iodine in volcanic fluids: ^{129}I results from the Central American Volcanic Arc. *Geochim. Cosmochim. Acta* **67**, 3827–3838.

Snyder G. T., Fehn U. and Goff F. (2002) Iodine isotope ratios and halide concentrations of the Satsuma-Iwojima volcano, Japan. *Earth Planets Space* **54**, 265–273.

Snyder G. T. and Fehn U. (2004) Global distribution of ^{129}I in rivers and lakes: implications for iodine cycling in surface reservoirs. *Nucl. Instr. Meth. B.* **223**(224), 579–586.

Snyder G. T. and Fabryka-Martin J. T. (2007) ^{129}I and ^{36}Cl in dilute hydrocarbon waters: marine-cosmogenic, in situ, and anthropogenic sources. *Appl. Geochem.* **22**, 692–714.

Snyder G. T., Riese R. C., Franks S., Fehn U., Pelzmann W. L., Gorody A. W. and Moran J. E. (2003) Origin and history of waters associated with coal bed methane: ^{129}I, ^{36}Cl, and stable isotope results from the Fruitland Formation. *CO and NM. Geochim. Cosmochim. Acta* **67**, 4529–4544.

Snyder G. T., Savov I. P. and Muramatsu Y. (2005) Iodine and boron in Mariana serpentinite mud volcanoes (ODP Legs 125 and 195): implications for forearc processes and subduction recycling. In: Shinohara, M., Salisbury, M.H. and Richter, C. (Eds.), Proc. Ocean Drilling Program, Scientific Results. Ocean Drilling Program, College Station, Texas. 1–18.

Snyder G., Aldahan A. and Possnert G. (2010) Global distribution and long term fate of anthropogenic I-129 in marine and surface water reservoirs. *Geochem. Geophy. Geosy.* **11**(4), Q04010.

Sillitoe R. H. and McKee E. H. (1996) Age of supergene oxidation and enrichment in the Chilean porphyry copper province. *Econ. Geol.* **91**, 164–179.

Singewald, Jr., J. T. and Miller B. L. (1916) The genesis of the Chilean nitrate deposits. *Econ. Geol.* **11**, 103–114.

Ullman W. J. and Aller R. C. (1983) Rates of iodine remineralization in terrigenous near-shore sediments. *Geochim. Cosmochim. Acta* **47**, 1423–1432.

Ullman W. J. and Aller R. C. (1985) The Geochemistry of iodine in near-shore carbonate sediments. *Geochim. Cosmochim. Acta* **49**, 967–978.

Vicente J. C. (2006) Dynamic Paleogeography of the Jurassic Andean Basin: pattern of regression and general considerations of main features. *Rev. Asoc. Geol. Argent.* **61**, 408–437.

Wetzel W. (1924) Petrographische Utersuchungen an chilenischen Salpetergesteinen. *Zeitschrift für praktische Geologie, Jahrg.* **32**(113–120), 132–142.

Wong G. T. F. (1991) The marine geochemistry of iodine. *Rev. Aquatic. Sci.* **4**, 45–73.

Young G. B. C., McElhiney J. E. and Paul G. W. (1991) An analysis of Fruitland coalbed methane production, Cedar Hill Field, Northern San Juan Basin. *Soc. Petrol. Eng.*, 263–276, Publication SPE22913.

Zhou J. and Lau K. M. (1998) Does a monsoon climate exist over South America. *J. Clim.* **11**, 1020–1040.

Associate editor: Brian W. Stewart